SUPPLEMENTAL INFORMATION

A Second-Generation Oral SARS-CoV-2 Main Protease Inhibitor Clinical Candidate for the Treatment of COVID-19

Authors: Charlotte M. N. Allerton[1], Joel T. Arcari[2], Lisa M. Aschenbrenner[2], Melissa Avery[2], Bruce M. Bechle[2], Mohammad Amin Behzadi[3], Britton Boras[4], Leanne M. Buzon[2], Rhonda D. Cardin[3], Natasha R. Catlin[2], Anthony A. Carlo[2], Karen J. Coffman[2], Alyssa Dantonio[2], Li Di[2], Heather Eng[2], Kathleen A. Farley[2], Rose Ann Ferre[4], Steven S. Gernhardt[2], Scott A. Gibson[5], Samantha E. Greasley[4], Siennah R. Greenfield[1], Brett L. Hurst[5], Amit S. Kalgutkar[1], Emi Kimito[2], Lorraine F. Lanyon[2], Gabrielle H. Lovett[1], Yajing Lian[2], Wei Liu[4], Luis A. Martínez Alsina[2], Stephen Noell[2], R. Scott Obach[2], Dafydd R. Owen[1]*, Nandini C. Patel[1], Devendra K. Rai[2], Matthew R. Reese[2], Hussin A. Rothan[3], Sylvie Sakata[4], Matthew F. Sammons[1], Jean G. Sathish[3], Raman Sharma[2], Claire M. Steppan[2], Jamison B. Tuttle[1], Patrick R. Verhoest[1], Liuqing Wei[2], Qingyi Yang[1], Irina Yurgelonis[3], Yuao Zhu[3]

Affiliations:

[1]Pfizer Research & Development; Cambridge, MA 02139, USA.

[2]Pfizer Research & Development; Groton, CT 06340, USA.

[3]Pfizer Research & Development; Pearl River, NY 10965, USA.

[4]Pfizer Research & Development; La Jolla, CA 92121, USA.

[5]Institute for Antiviral Research, Department of Animal, Dairy, and Veterinary Sciences, Utah State University; Logan, UT 84322, USA.

*Corresponding author. Email: dafydd.owen@pfizer.com

Table of Contents

Protein Reagent Preparation

Recombinant SARS-CoV-2 M^{pro} Protease Production

Purification of SARS-CoV-2 M^{pro}

Purification of SARS-CoV-2 M^{pro} +G

Generation of Assay Ready Plates for Coronavirus M^{pro} and Mammalian Protease Assays

Crystallization and Structure Determination

Table S1 Diffraction Data and Refinement Statistics for **9**

Table S2 Biochemical Determination for Human Coronavirus M^{pro} Assays

Table S3 Mammalian Protease Panel: Peptide Sequences and Reagent Parameters

Table S4 Selectivity of PF-07817883 against a panel of mammalian proteases and HIV1 protease.

Data Analysis for Mammalian and Coronavirus Protease Panels

Disposition Studies Methods

Metabolism of Compound **9** in Human Liver Microsomes and Human Hepatocytes.

Ultrahigh Performance Liquid Chromatography (UHPLC)-High Resolution Mass Spectrometry for Metabolite Profiling

Biosynthesis of Metabolites M1 and M2 of Compound **9**

Determination of the $CL_{int,app}$ for **9** in HLM

Pharmacokinetics Studies Methods

Rat Pharmacokinetics

Monkey Pharmacokinetics

NMR Spectra of biologically tested compounds

^{1}H Spectrum of compound **4** in dimethyl sulfoxide-d_6 at 27^{o}C.

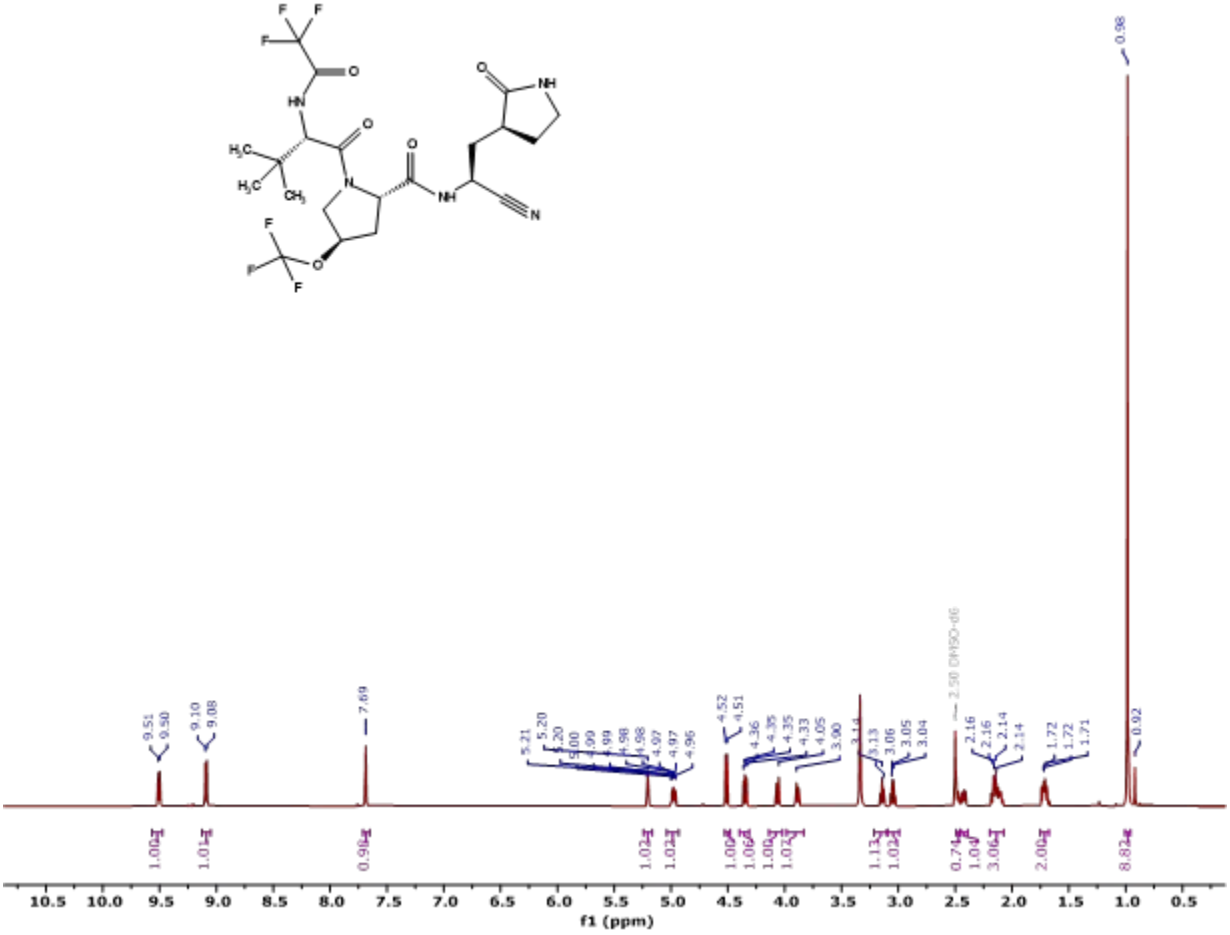

^{13}C Spectrum of compound **4** in dimethyl sulfoxide-d_6 at 27^{o}C.

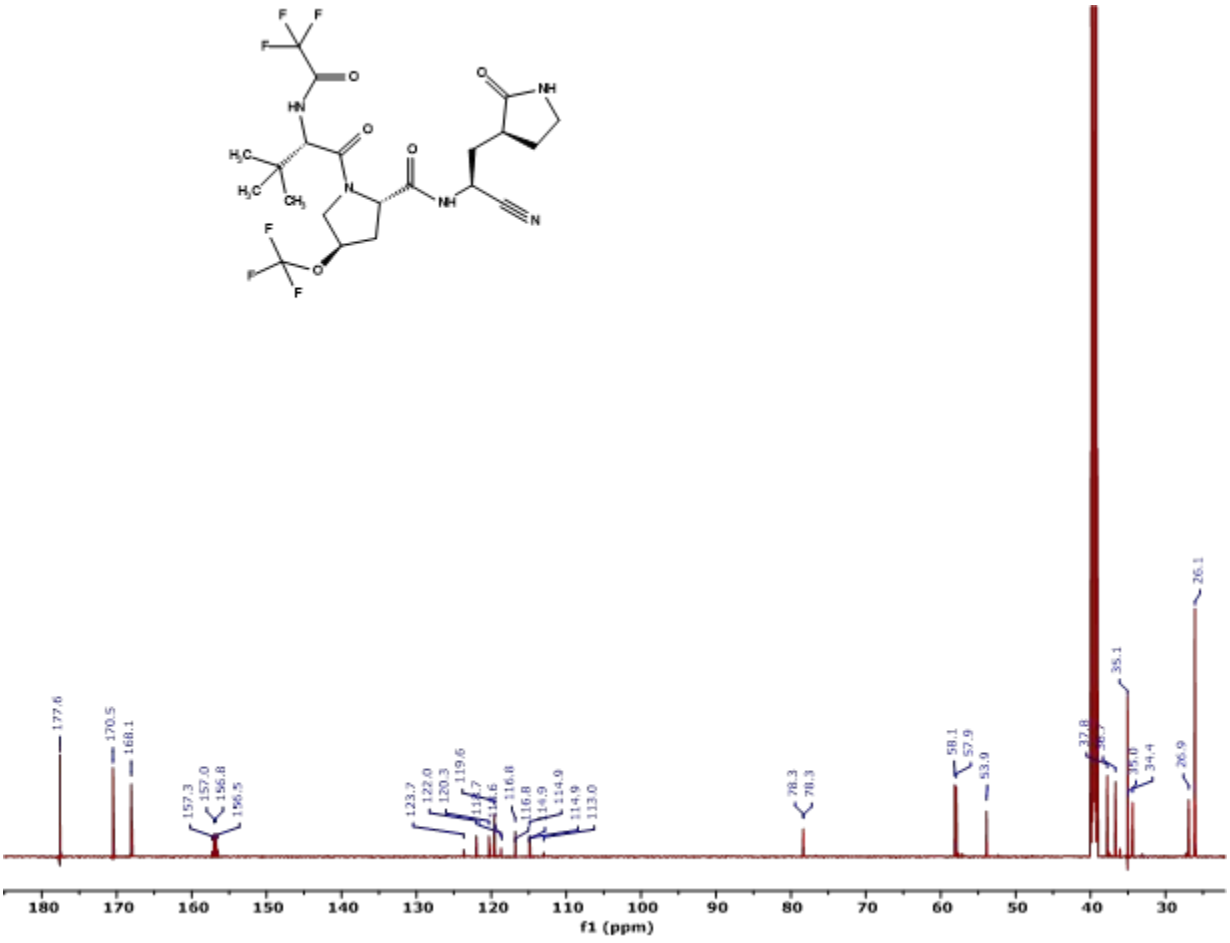

^{19}F Spectrum of compound **4** in dimethyl sulfoxide-d_6 at 27^{o}C.

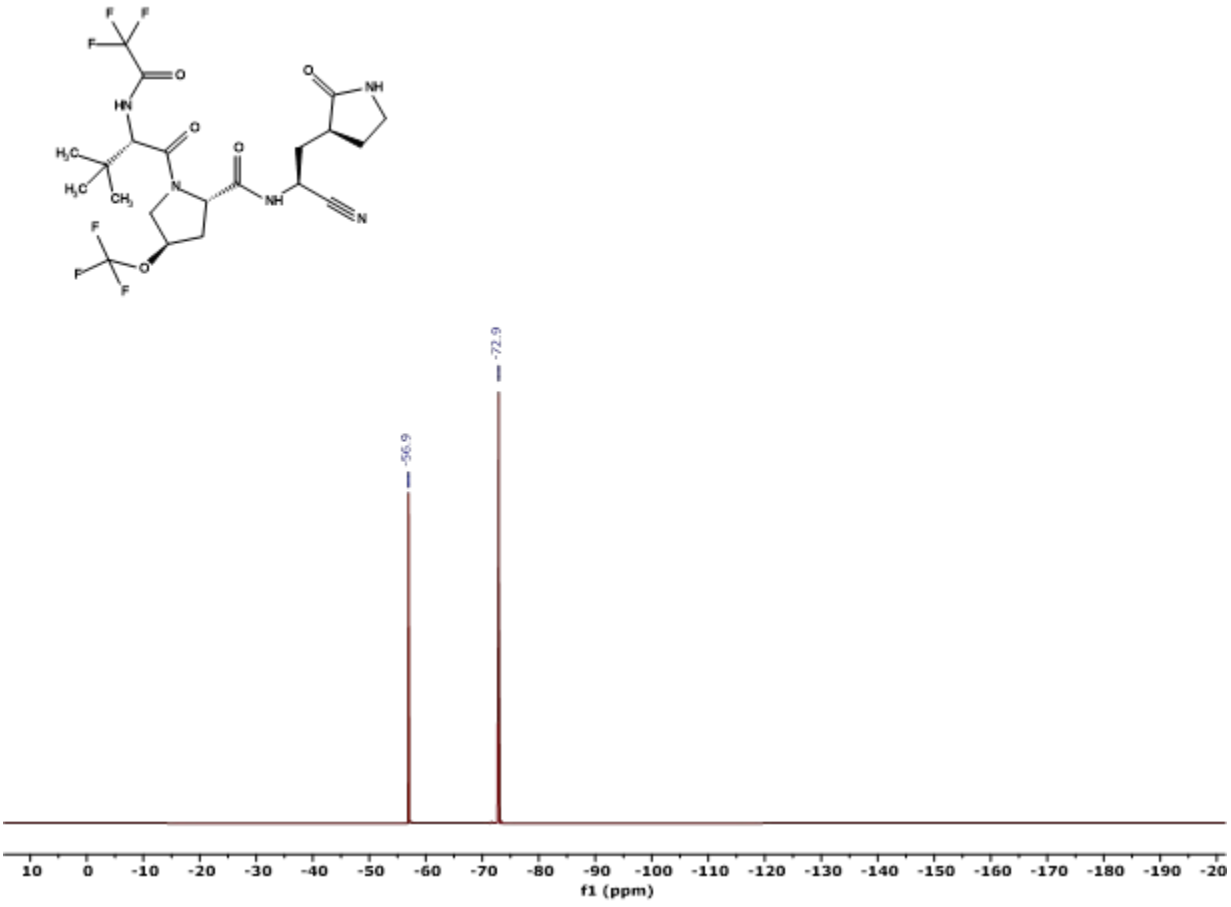

^{1}H Spectrum of compound **5** in dimethyl sulfoxide-d_6 at 27^{o}C.

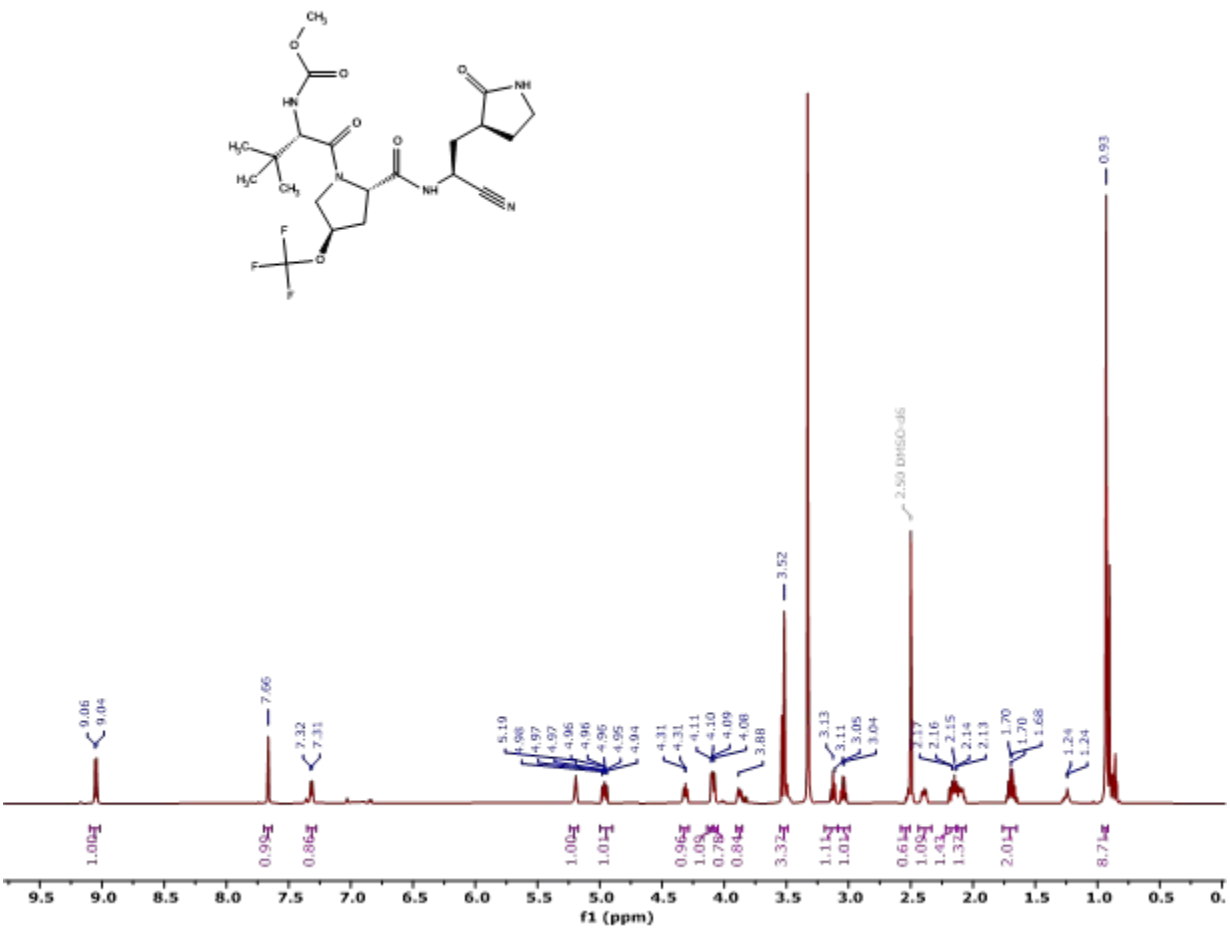

^{13}C Spectrum of compound **5** in dimethyl sulfoxide-d_6 at 27^{o}C.

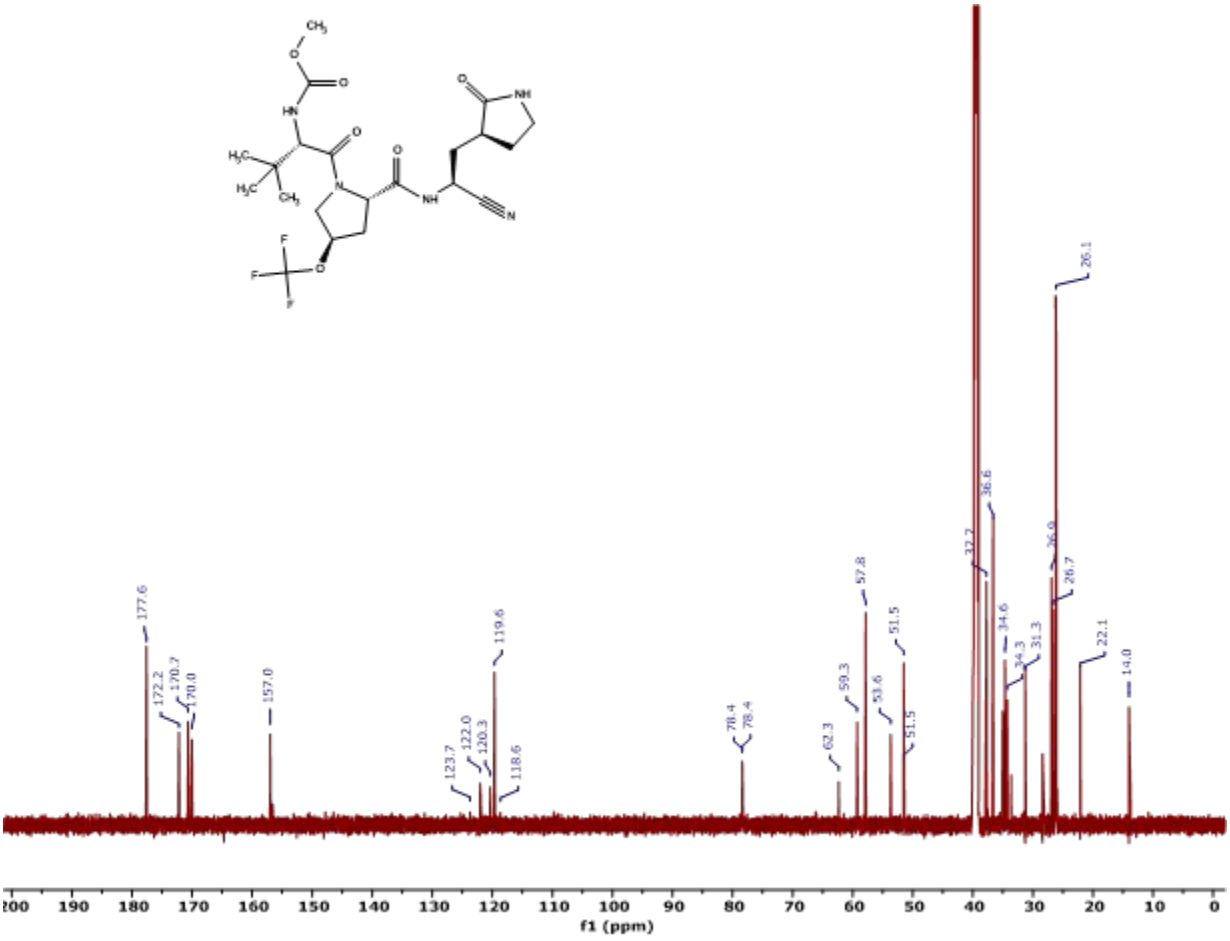

^{19}F Spectrum of compound **5** in dimethyl sulfoxide-d_6 at 27^{o}C.

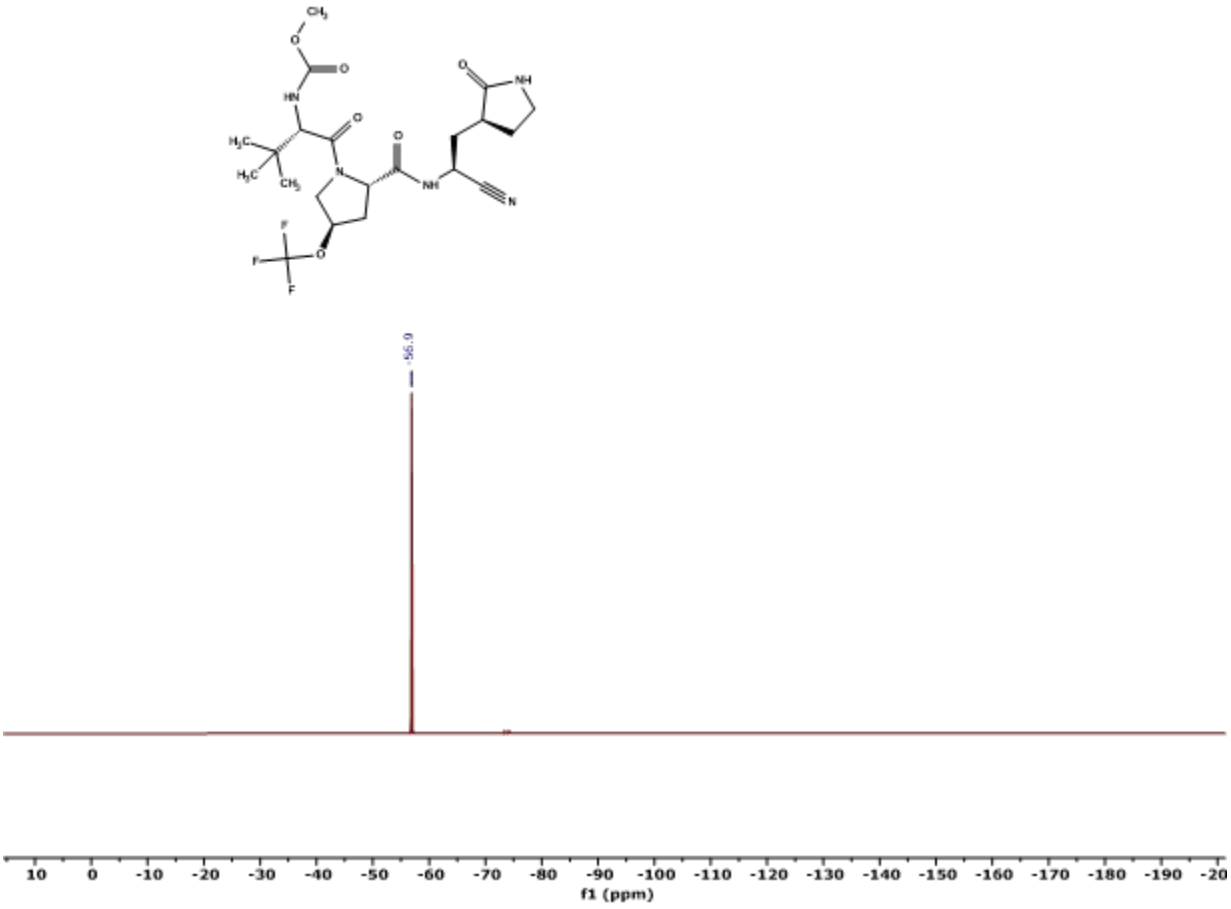

^{1}H Spectrum of compound **6** in dimethyl sulfoxide-d_6 at 27^{o}C.

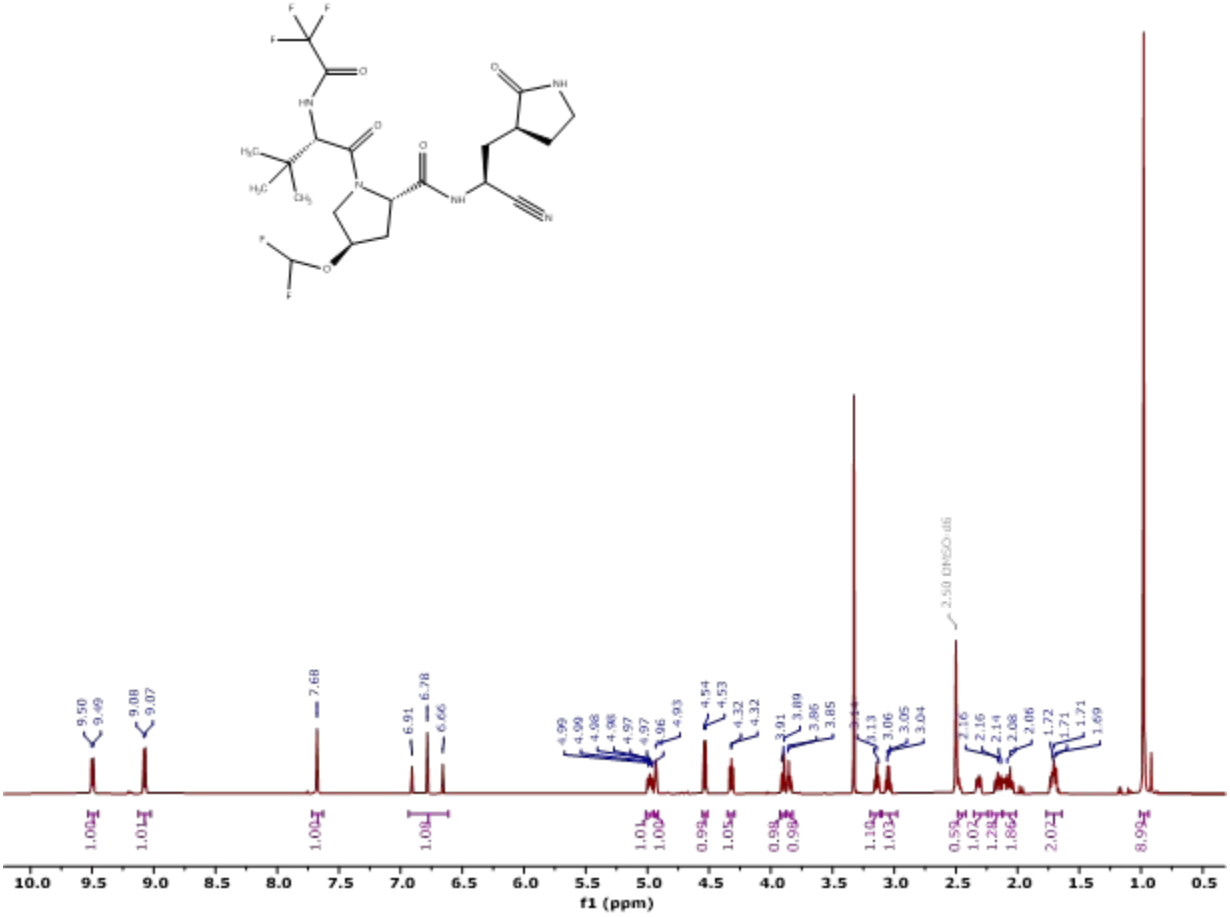

^{13}C Spectrum of compound **6** in dimethyl sulfoxide-d_6 at 27°C.

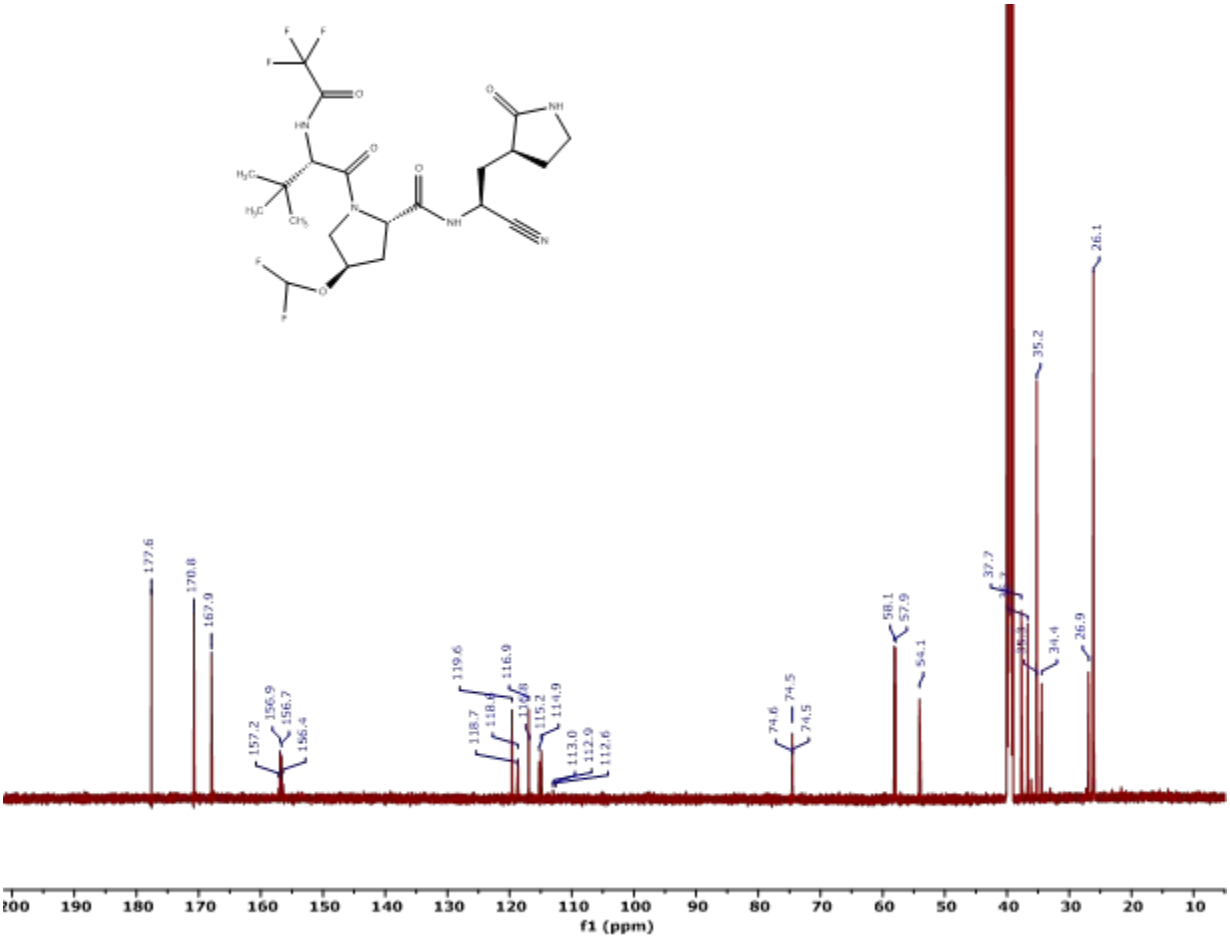

^{19}F Spectrum of compound **6** in dimethyl sulfoxide-d_6 at 27°C.

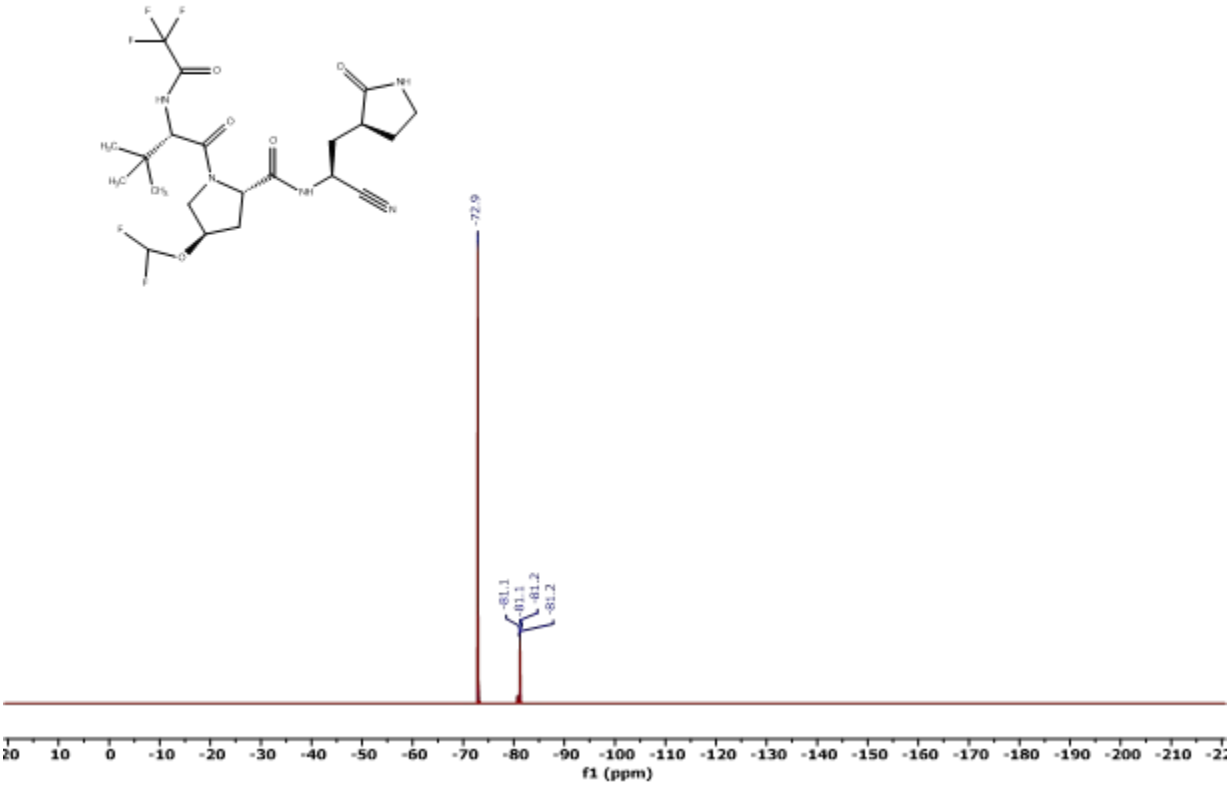

^{1}H Spectrum of compound **7** in dimethyl sulfoxide-d_6 at 27^{o}C.

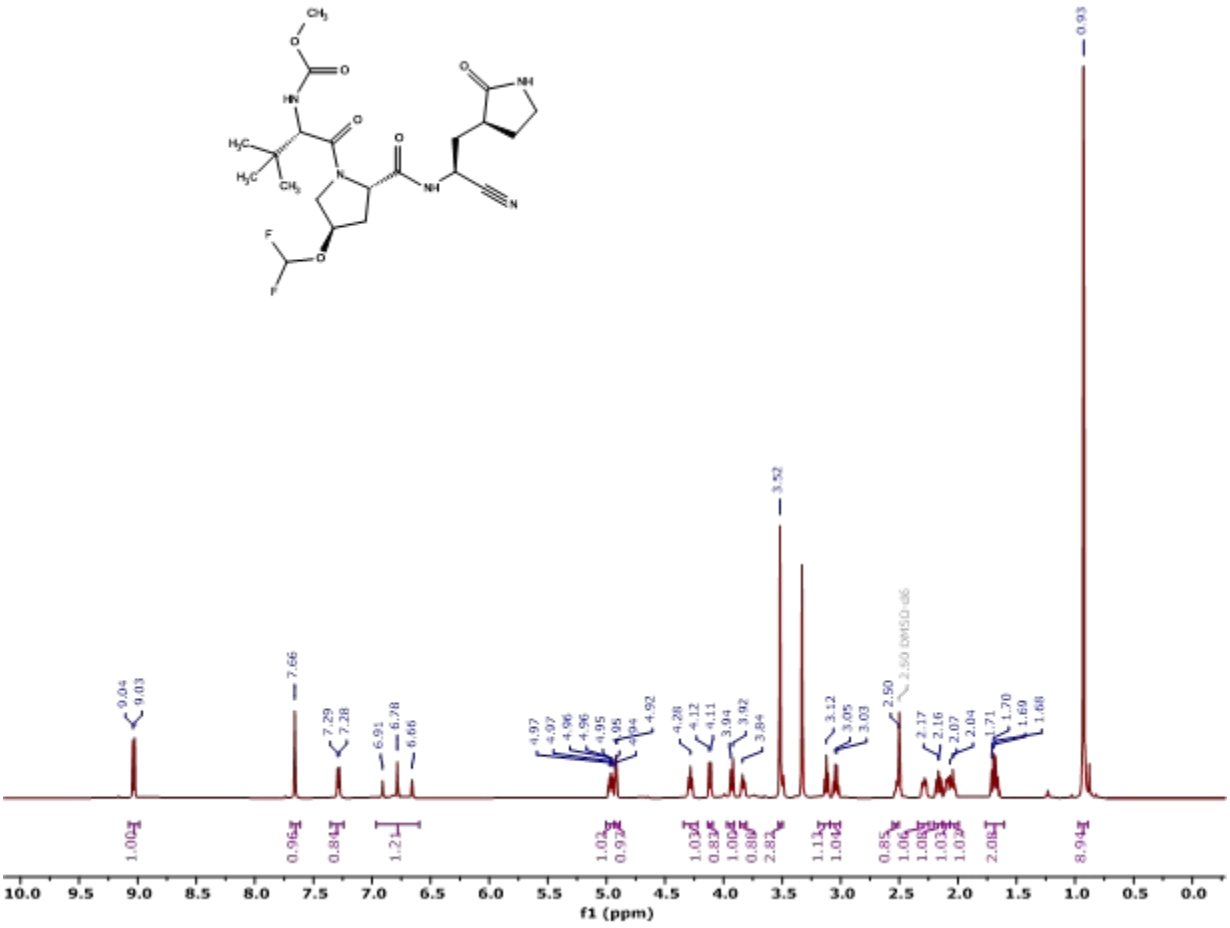

^{13}C Spectrum of compound **7** in dimethyl sulfoxide-d_6 at 27^{o}C.

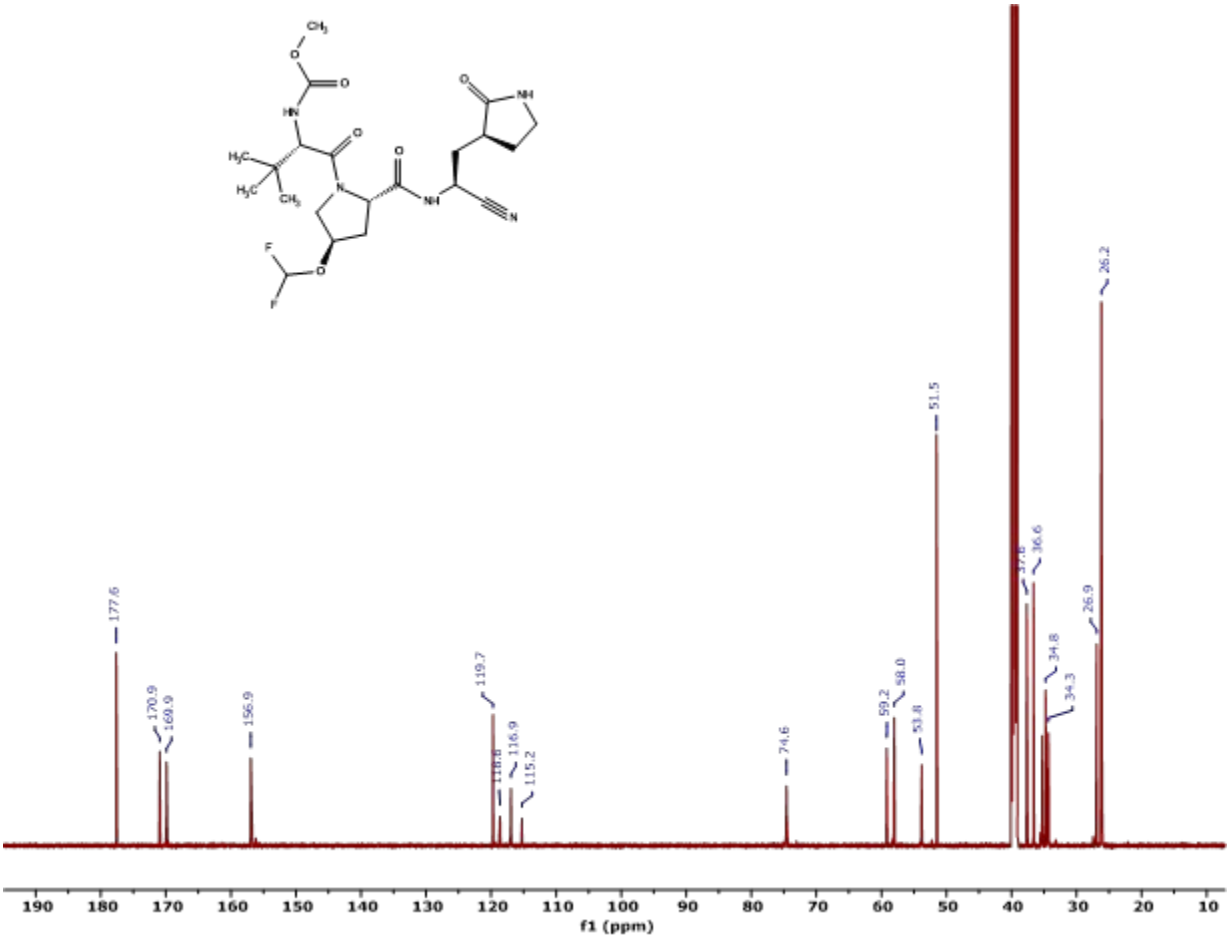

^{19}F Spectrum of compound **7** in dimethyl sulfoxide-d_6 at 27°C.

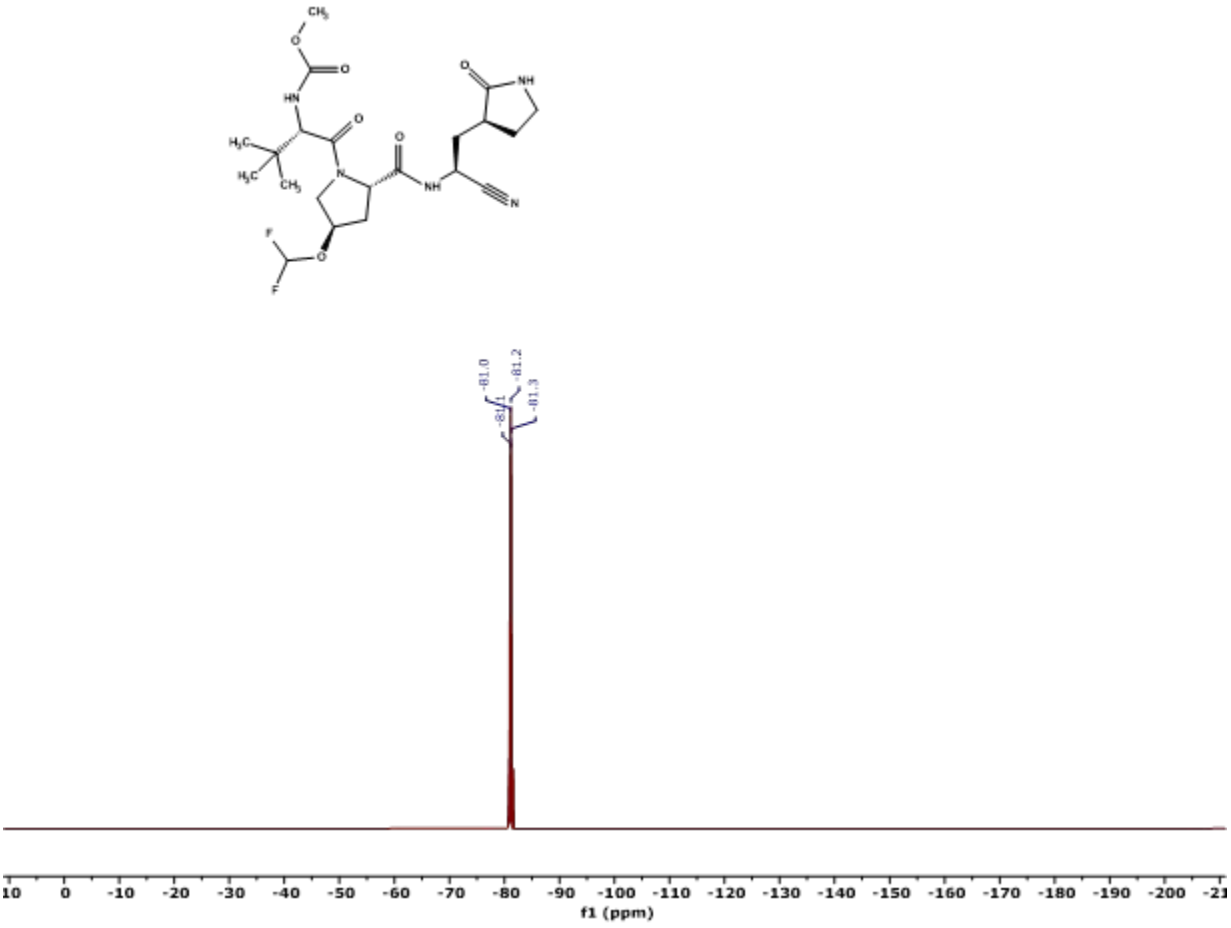

^{1}H Spectrum of compound **8** in dimethyl sulfoxide-d_6 at 27^{o}C.

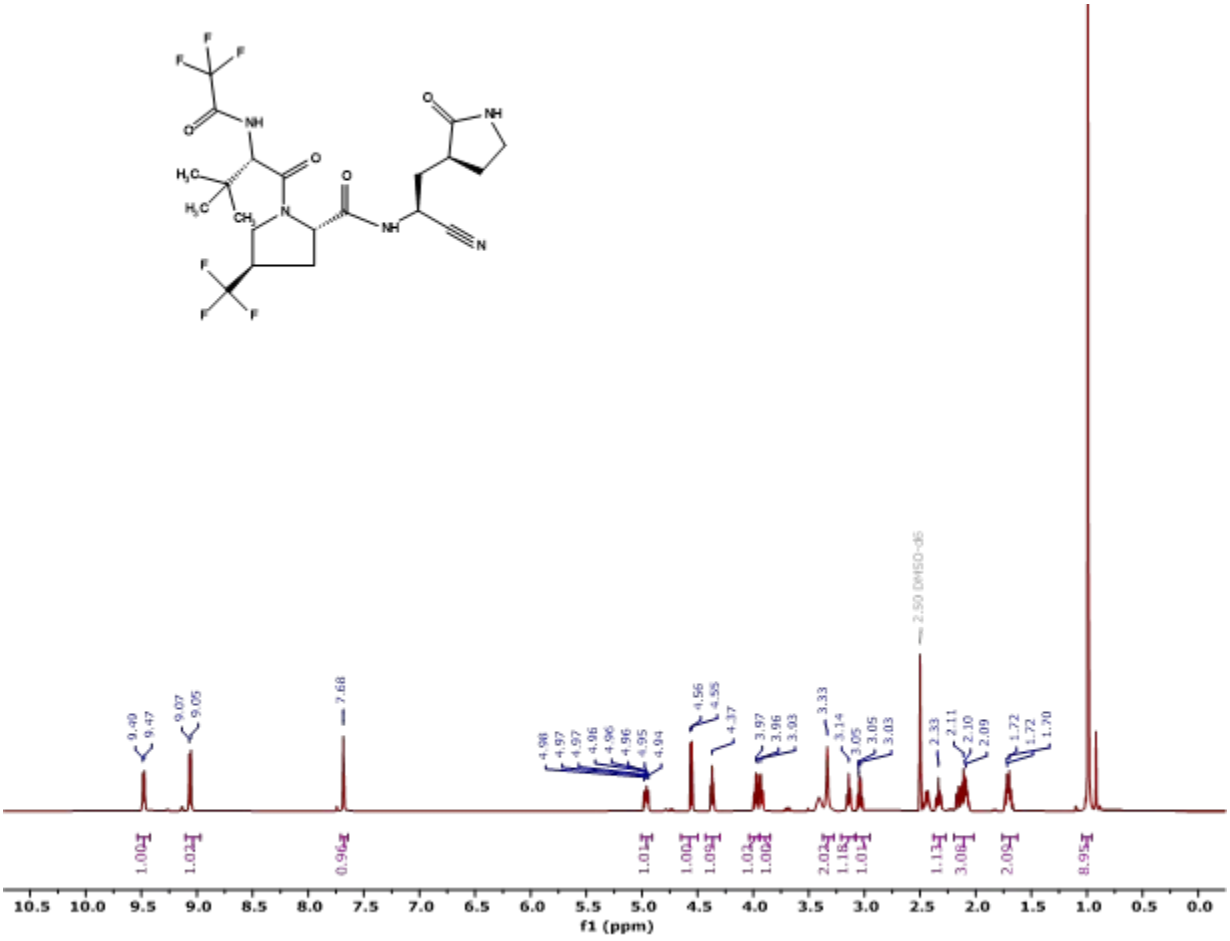

^{13}C Spectrum of compound **8** in dimethyl sulfoxide-d_6 at 27^{o}C.

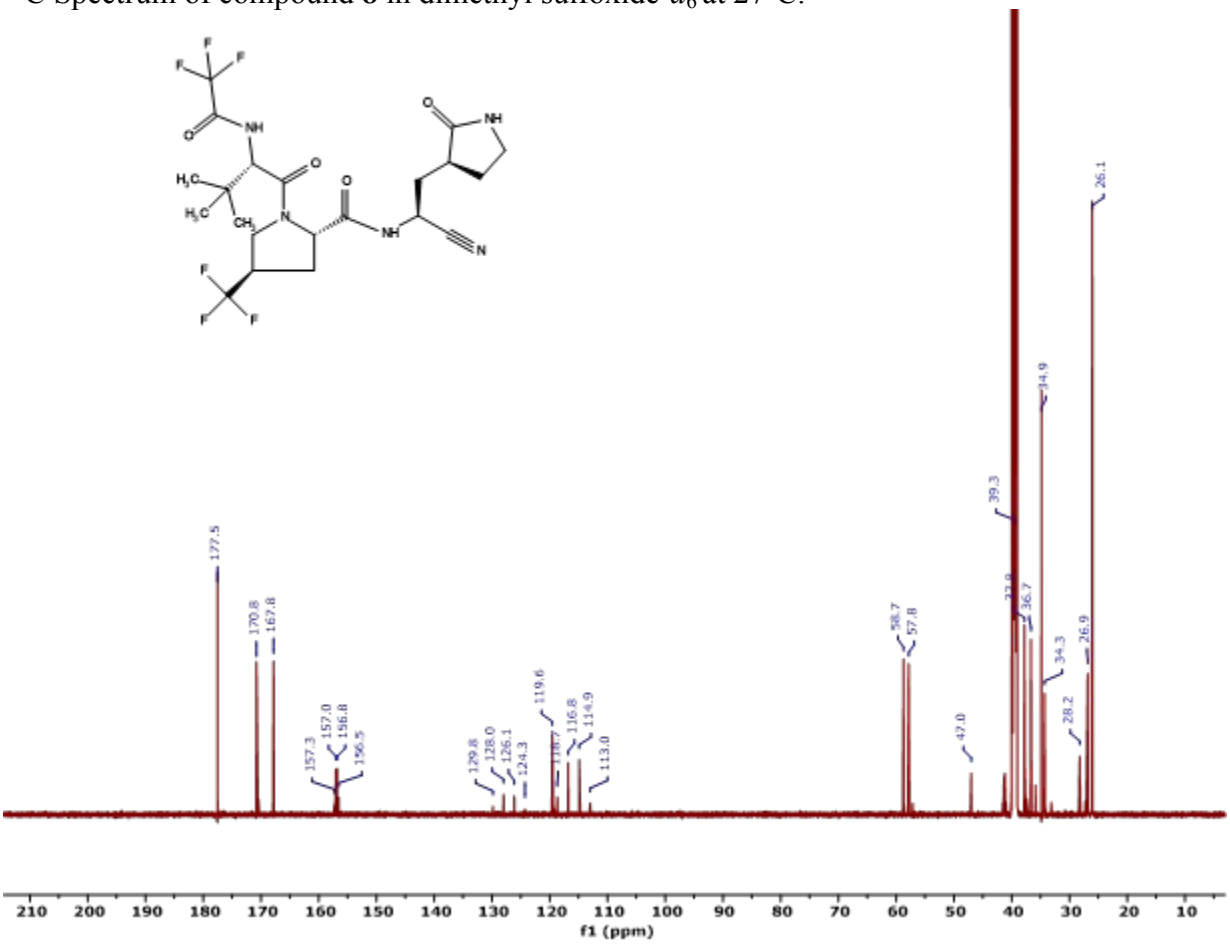

^{19}F Spectrum of compound **8** in dimethyl sulfoxide-d_6 at 27°C.

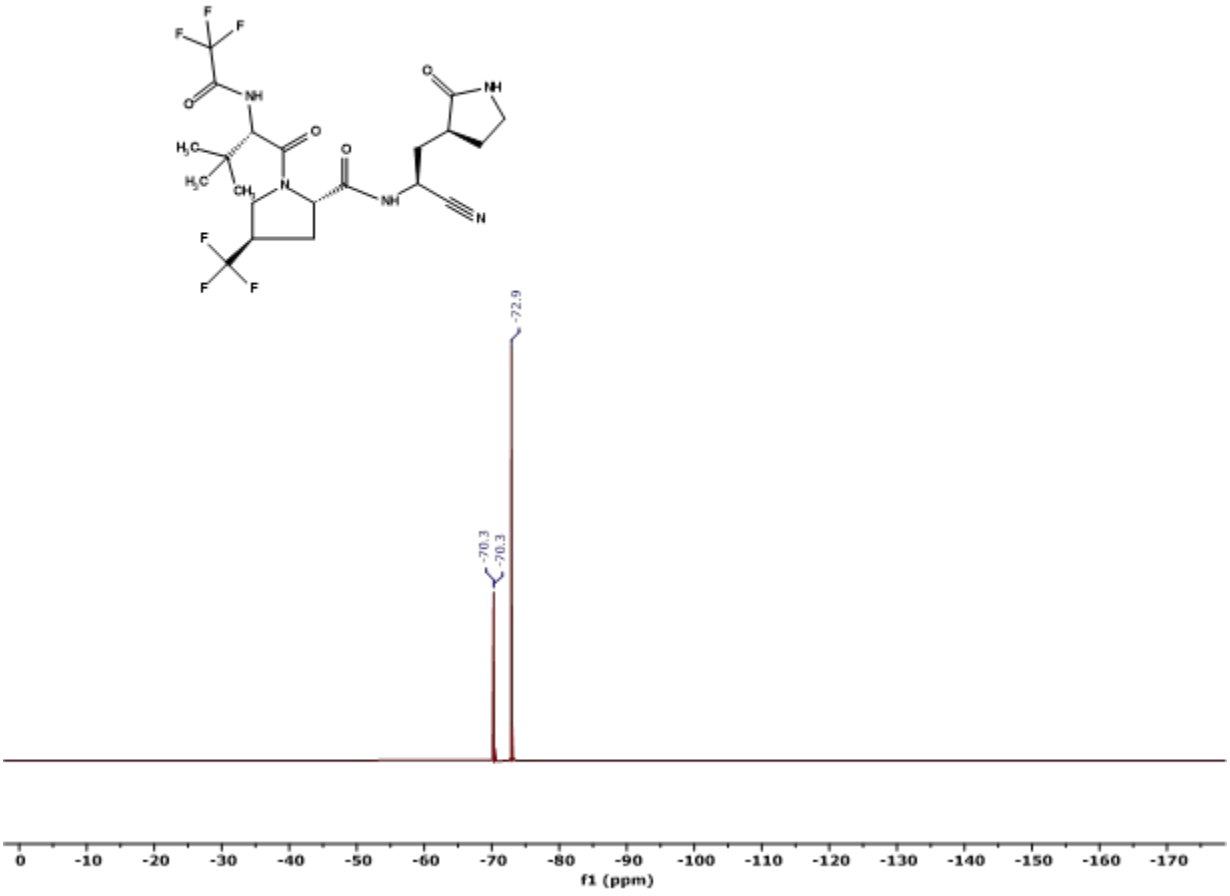

Assigned ^{1}H Spectrum of compound **9** in dimethyl sulfoxide-d_6 at 27^{o}C.

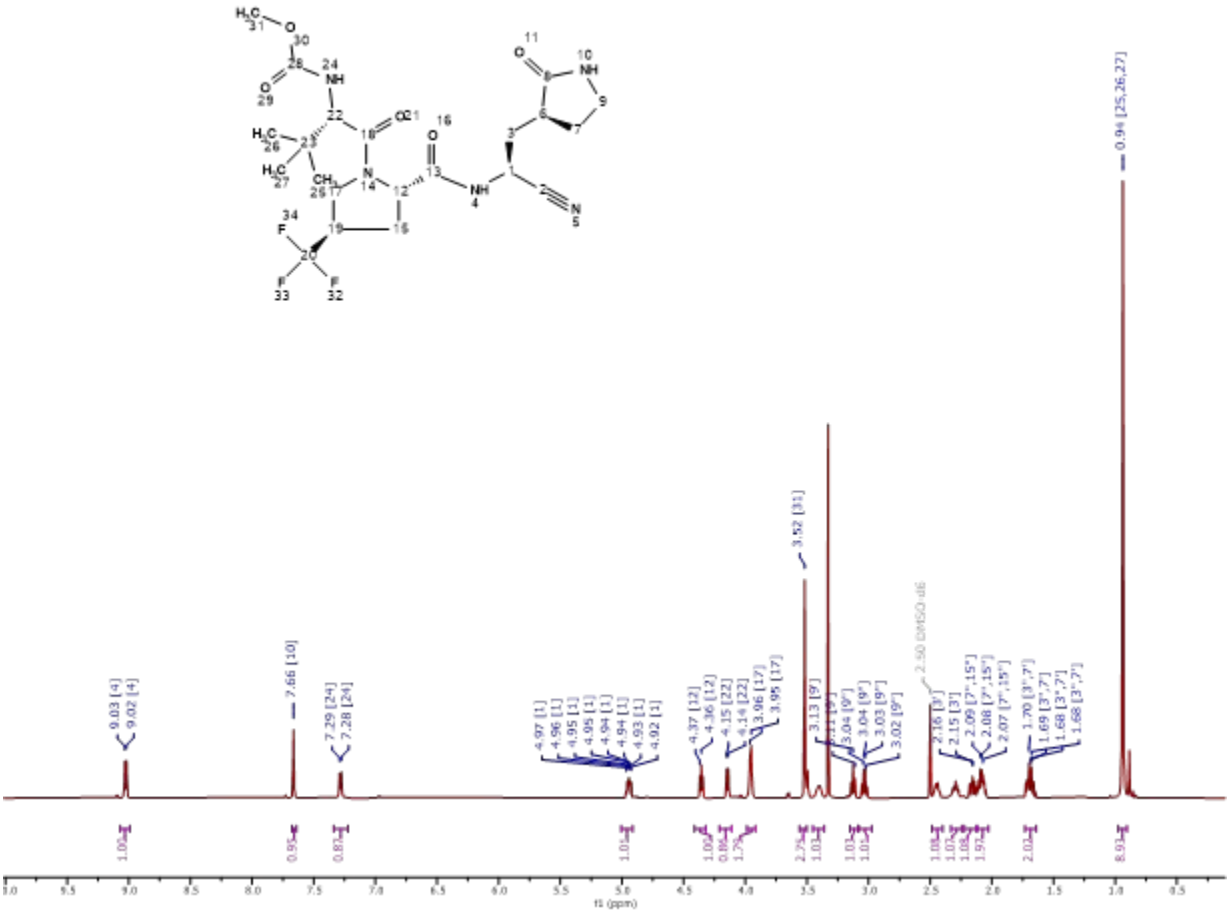

Assigned ^{13}C Spectrum of compound **9** in dimethyl sulfoxide-d_6 at 27°C.

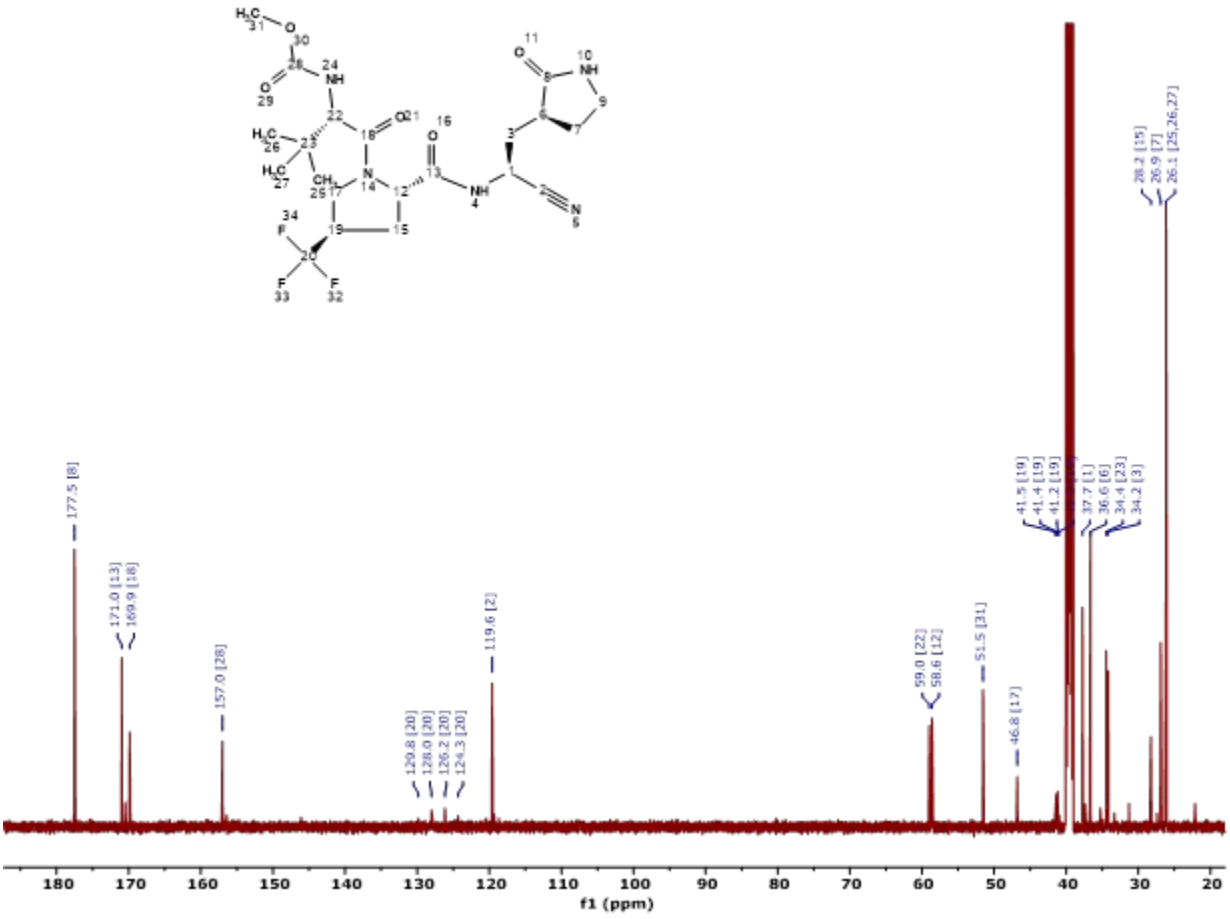

Assigned ^{19}F Spectrum of compound **9** in dimethyl sulfoxide-d_6 at 27°C.

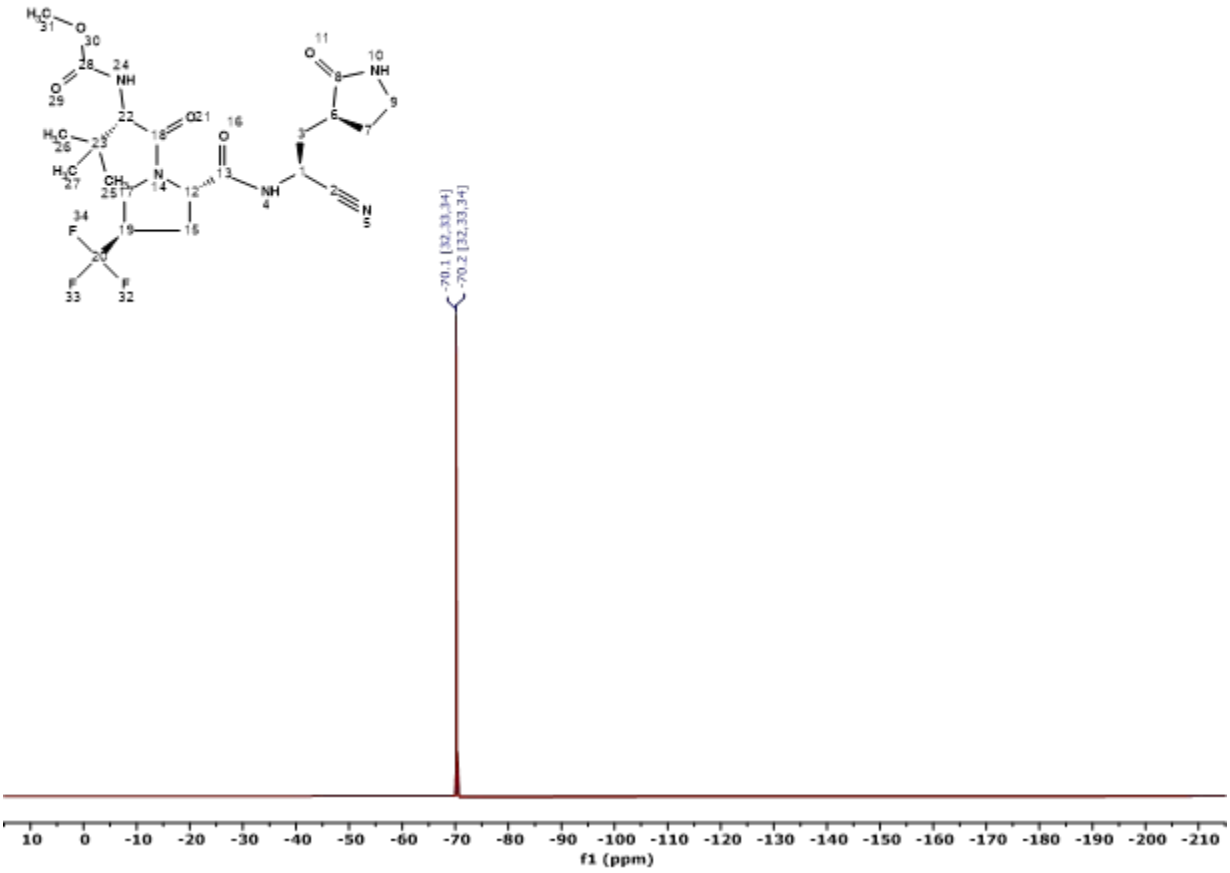

^{1}H Spectrum of compound **10** in dimethyl sulfoxide-d_6 at 27^{o}C.

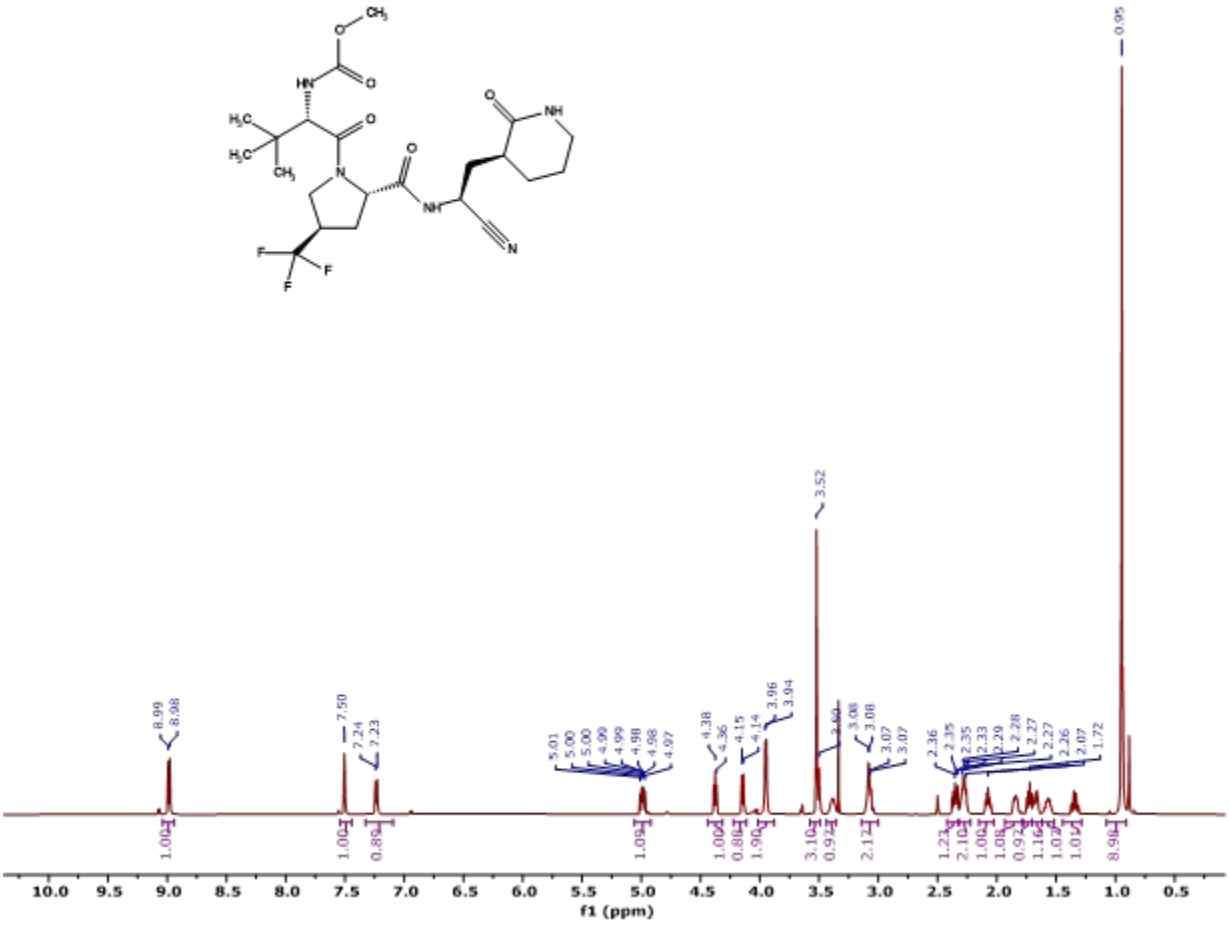

^{13}C Spectrum of compound **10** in dimethyl sulfoxide-d_6 at 27°C.

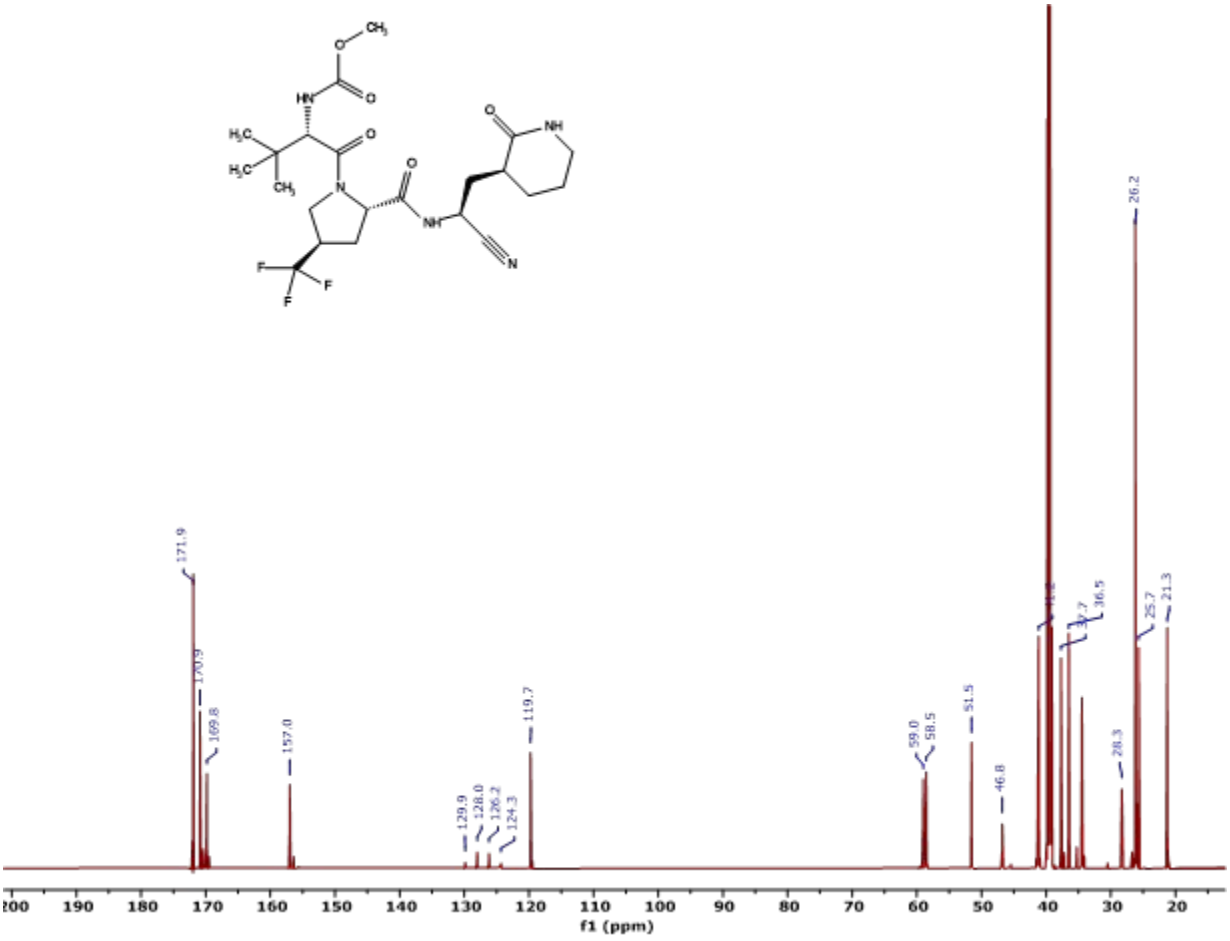

^{19}F Spectrum of compound **10** in dimethyl sulfoxide-d_6 at 27^{o}C.

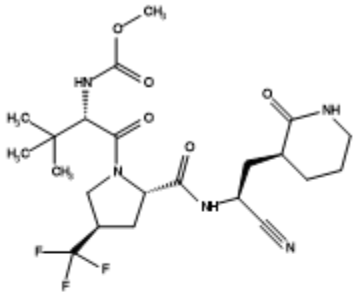

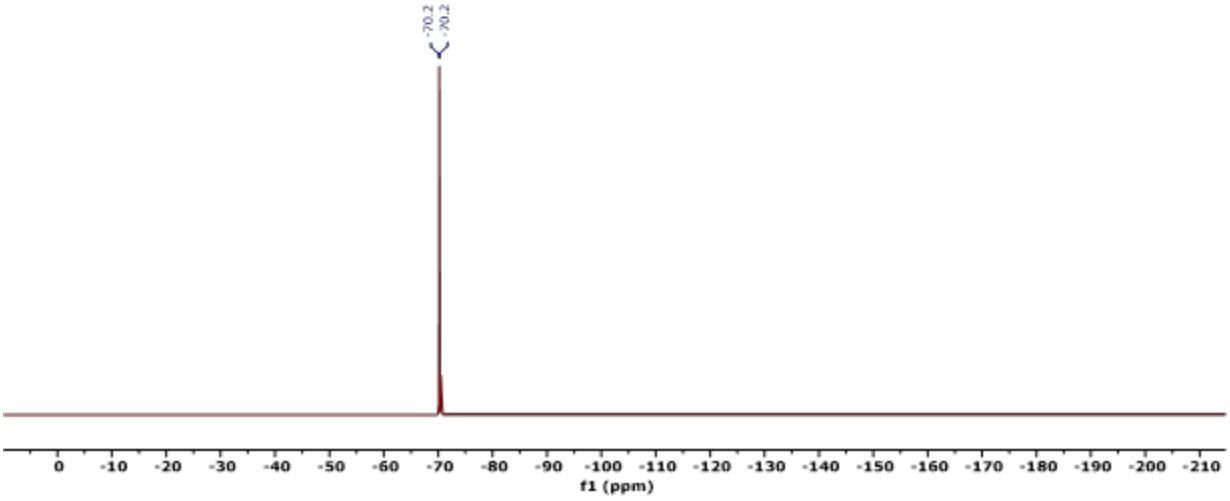

^{1}H Spectrum of compound **11** in dimethyl sulfoxide-d_6 at 27^{o}C.

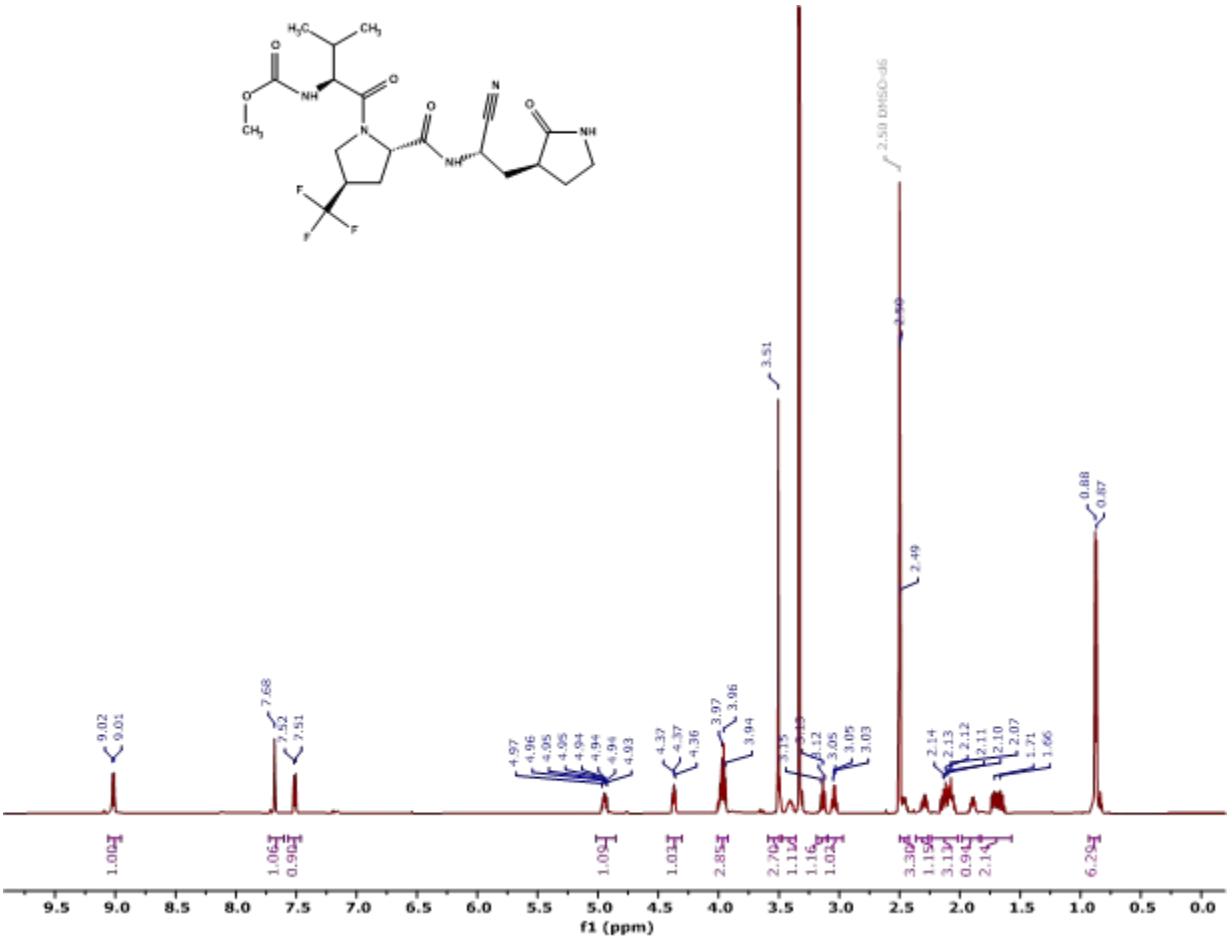

^{13}C Spectrum of compound **11** in dimethyl sulfoxide-d_6 at 27°C.

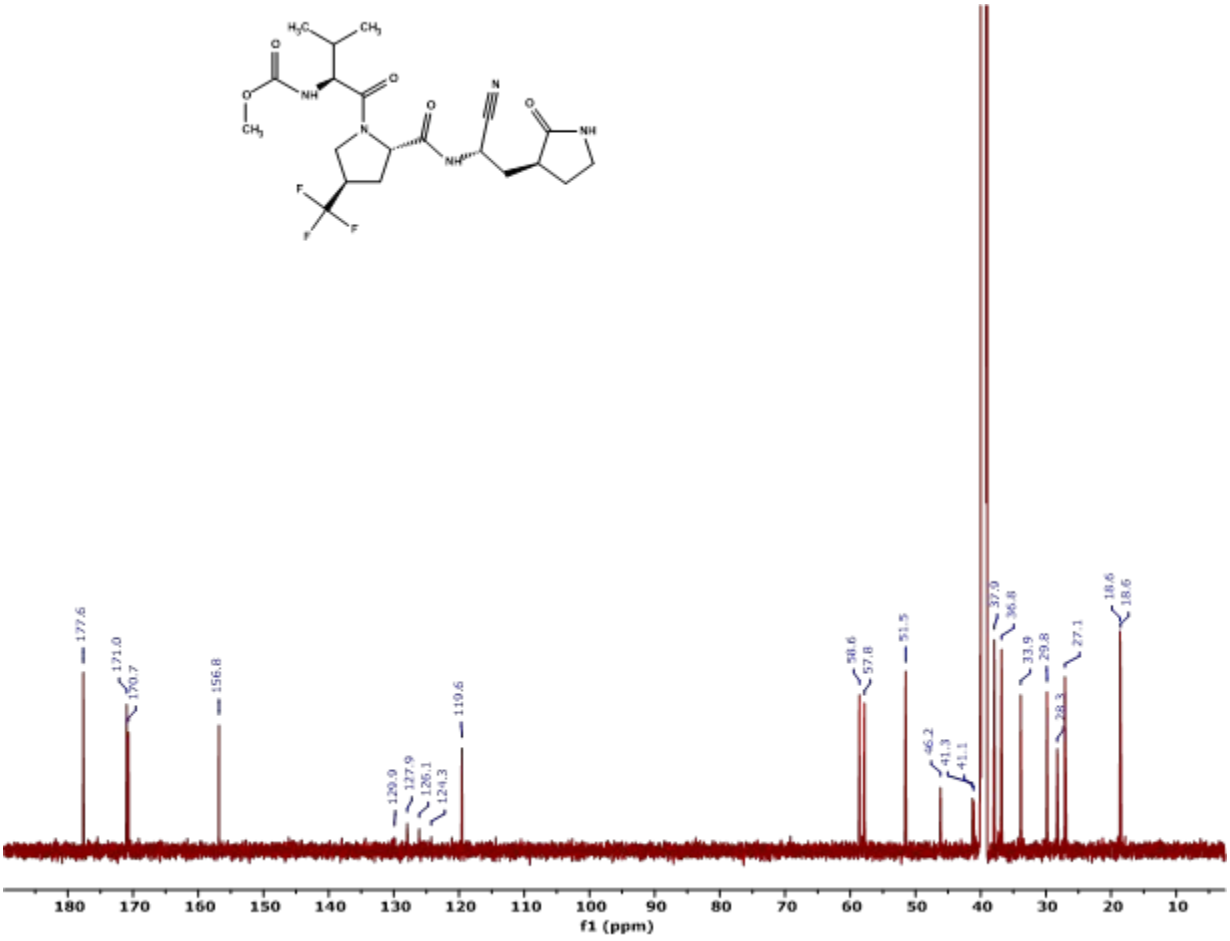

^{19}F Spectrum of compound **11** in dimethyl sulfoxide-d_6 at 27^{o}C.

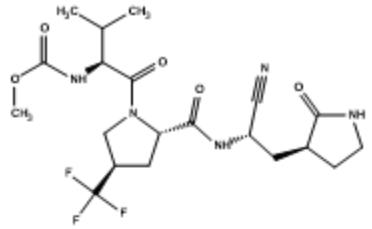

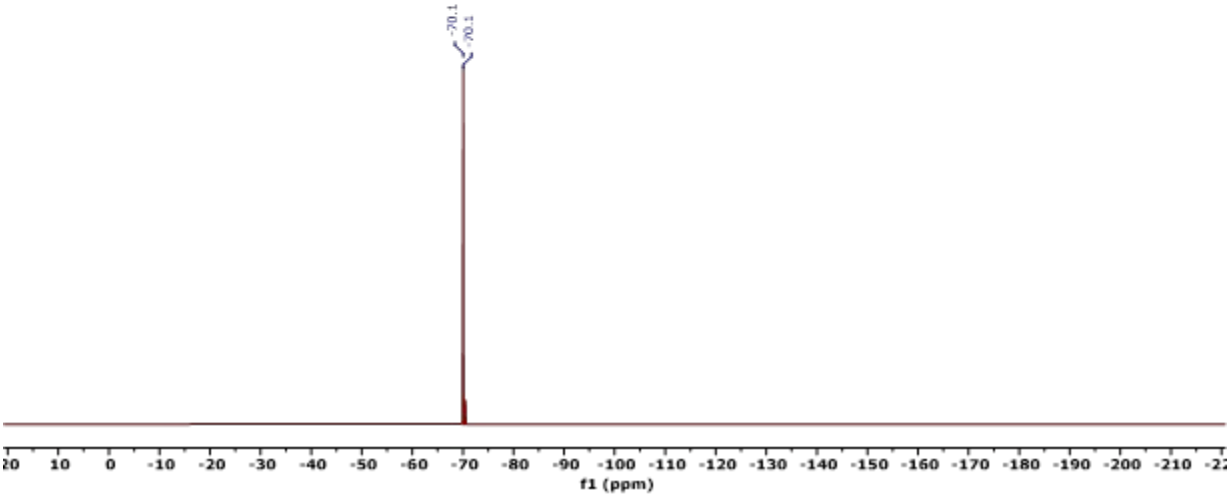

^{1}H Spectrum of compound **12** in dimethyl sulfoxide-d_6 at 27^{o}C.

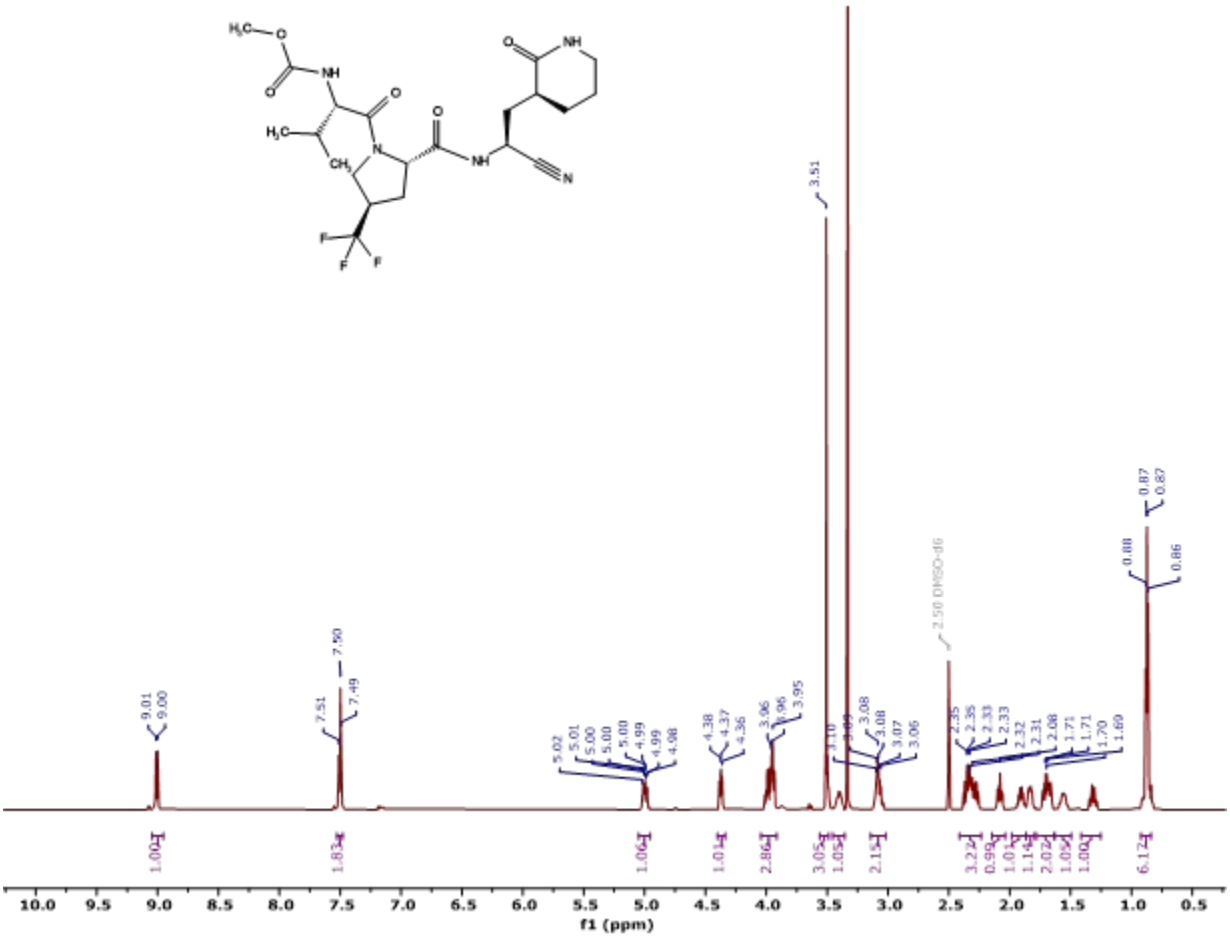

^{13}C Spectrum of compound **12** in dimethyl sulfoxide-d_6 at 27°C.

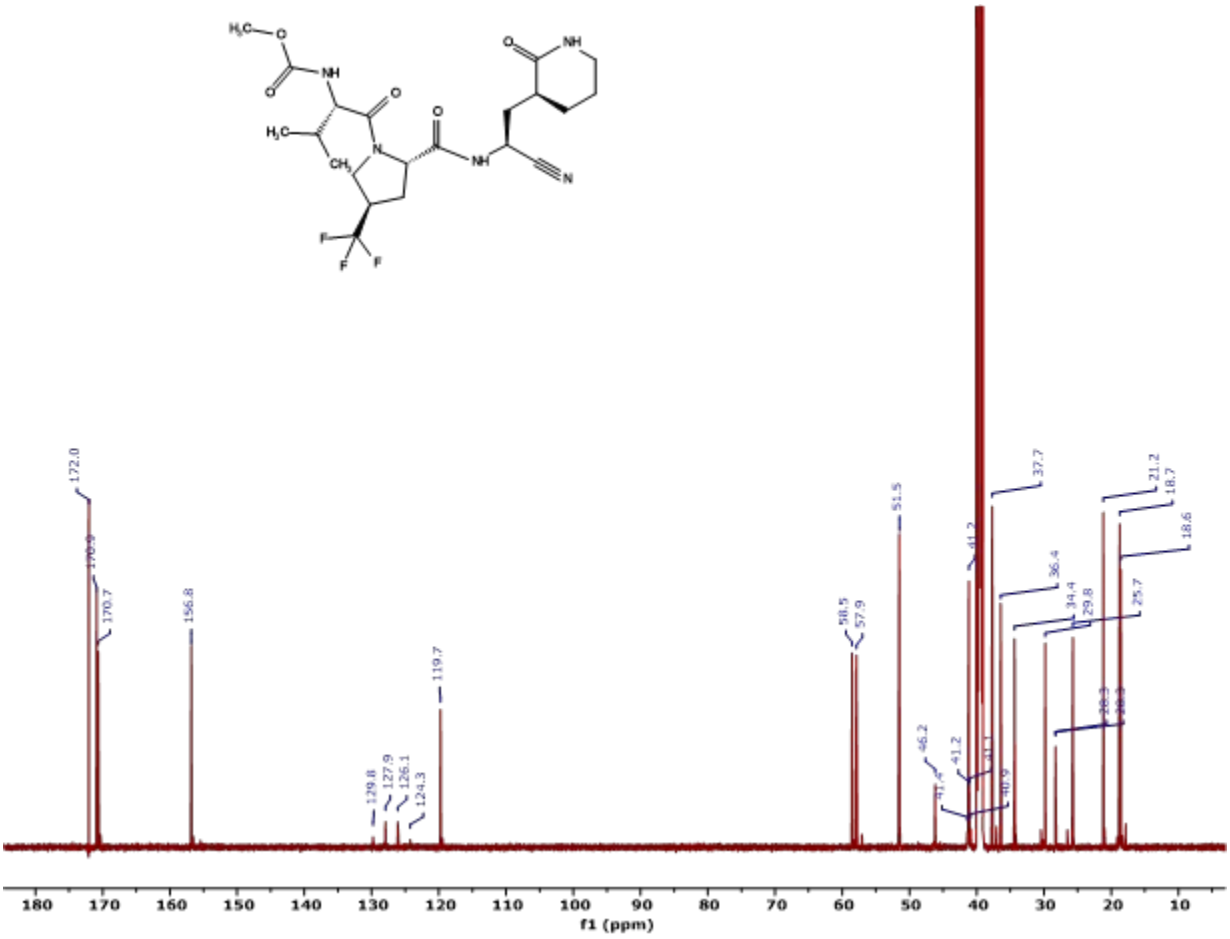

^{19}F Spectrum of compound **12** in dimethyl sulfoxide-d_6 at 27^{o}C.

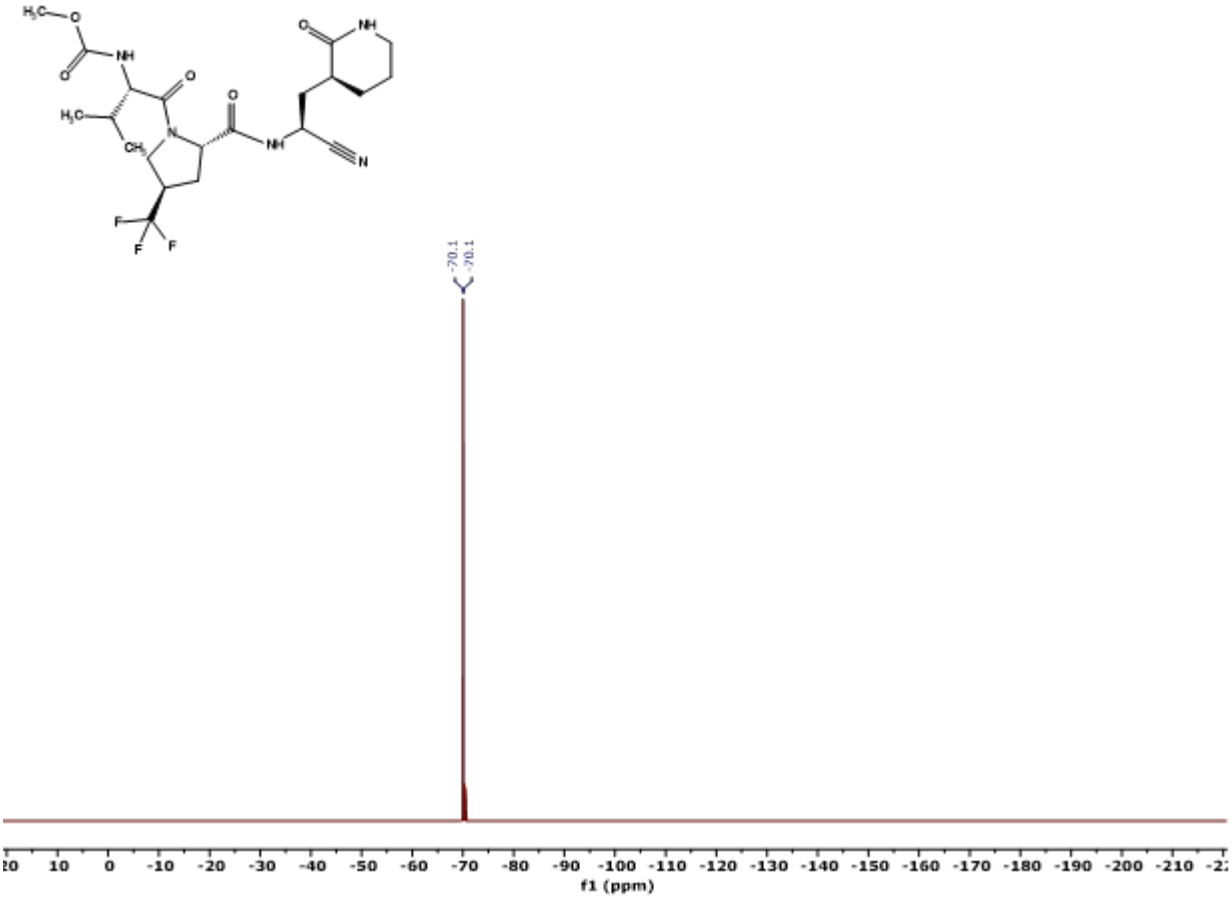

HPLC analysis of compound **9** showing >99% purity of amorphous material post synthesis and purification

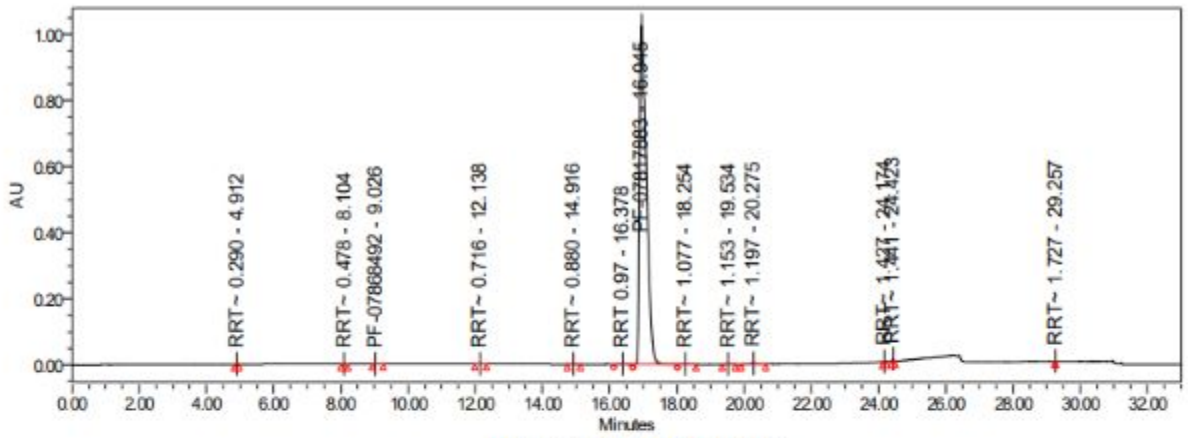

SampleName PF-07817883-00-0014

	Name	RT	RRT_Alpha	Area	Height (µV)	% Area (Total All Peaks)	Impurity_PFE	USP s/n	USP Resolution	USP Plate Count
1	RRT~ 0.290	4.912	0.290	2444.97	797	0.02	0.02	27.397966		5.520671e+004
2	RRT~ 0.478	8.104	0.478	2167.78	496	0.01	0.01	16.689298	3.254852e+001	8.305022e+004
3	PF-07868492	9.026	0.533	2490.32	403	0.02	0.02	13.353443	7.741249e+000	8.223559e+004
4	RRT~ 0.716	12.138	0.716	1976.77	262	0.01	0.01	8.331432	2.094615e+001	8.046038e+004
5	RRT~ 0.880	14.916	0.880	3222.33	345	0.02	0.02	11.305949	1.335169e+001	5.927553e+004
6	RRT 0.97	16.378	0.967	8623.65	803	0.06	0.06	27.625235	5.619045e+000	5.671345e+004
7	PF-07817883	16.945	1.000	14418434.95	1024430	99.41		36518.489510	1.700358e+000	2.993478e+004
8	RRT~ 1.077	18.254	1.077	12410.50	939	0.09	0.09	32.470173	3.571036e+000	4.572649e+004
9	RRT~ 1.153	19.534	1.153	1137.86	101	0.01	0.01	2.612398	6.392008e+000	1.745267e+006
10	RRT~ 1.197	20.275	1.197	35466.24	2502	0.24	0.24	88.191448	3.411895e+000	4.676731e+004
11	RRT~ 1.427	24.174	1.427	1728.68	872	0.01	0.01	30.074147	1.823670e+001	3.379478e+006
12	RRT~ 1.441	24.423	1.441	11938.83	7291	0.08	0.08	258.917306	5.160391e+000	4.963966e+006
13	RRT~ 1.727	29.257	1.727	1308.02	2209	0.01	0.01	77.744898	1.589458e+002	4.750874e+007

	USP Tailing
1	9.149365e-001

	USP Tailing
2	1.054479e+000

	USP Tailing
3	1.848978e+000

	USP Tailing
4	1.115460e+000

	USP Tailing
5	1.094762e+000

	USP Tailing
6	1.083990e+000

	USP Tailing
7	2.109847e+000
8	
9	1.009176e+000
10	1.054572e+000
11	6.990717e-001
12	9.724240e-001
13	1.015850e+000

HPLC analysis of compound **9** showing >99% purity of amorphous material post 75% loaded spray dried dispersion preparation. This was the material used *in vivo*.

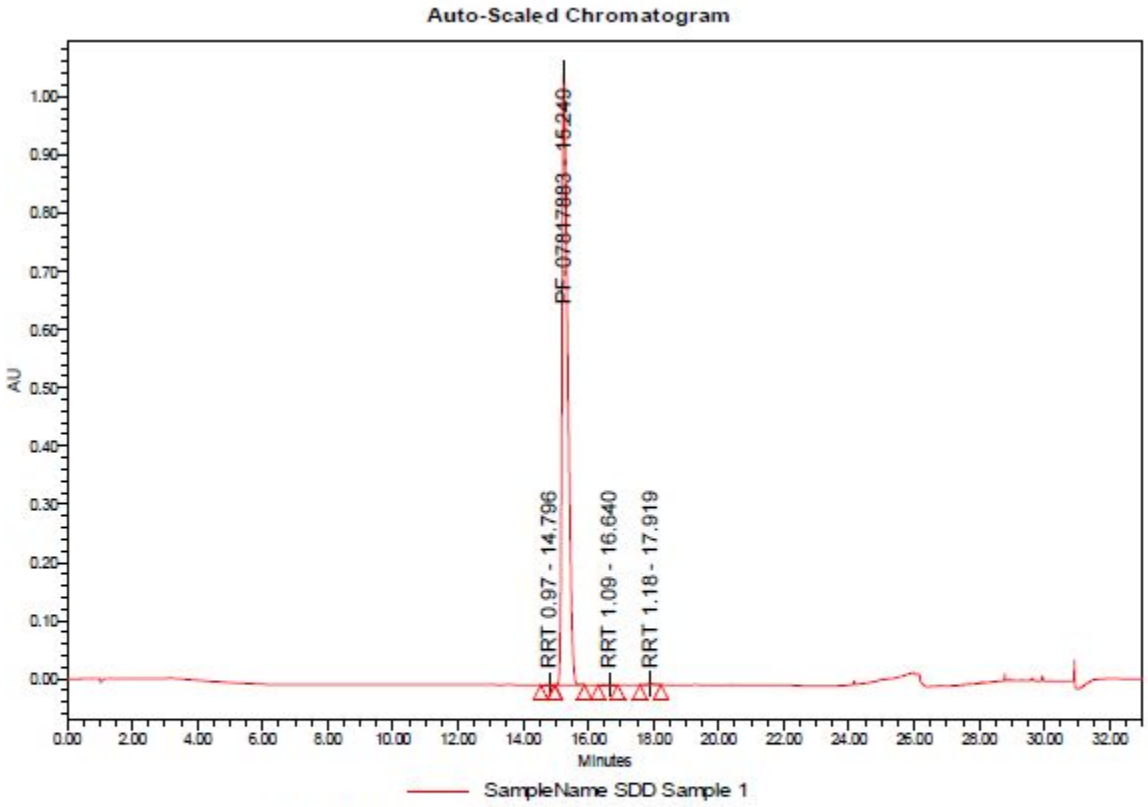

Sample Name: SDD Sample 1

	Peak Name	Result Id	Retention Time (min)	RRT	Area	Height	Impurity Level	USP Resolution	Imp_Calc
1	RRT 0.97	109405	14.796	0.970	7004	710	0.06		Area % Parent
2	PF-07817883	109405	15.249	1.000	12710264	1052488		1.5	Area % Parent
3	RRT 1.09	109405	16.640	1.091	9903	690	0.08	3.8	Area % Parent
4	RRT 1.18	109405	17.919	1.175	30530	1974	0.24	3.1	Area % Parent
Sum							0.4		

Figure S1. The ^{1}H spectra of compound **9** in dimethyl sulfoxide-d_6 with increasing temperature. At room temperature, many of the resonances have restricted rotation and are observed as two distinct resonances (94:6 rotamer). At 140°C, the rotation is no longer restricted and the resonances appear as a single peak. For example, the resonances at 7.7 and 7.6 ppm observed at 27°C coalesce to a single resonance at 7.2 ppm at 140°C.

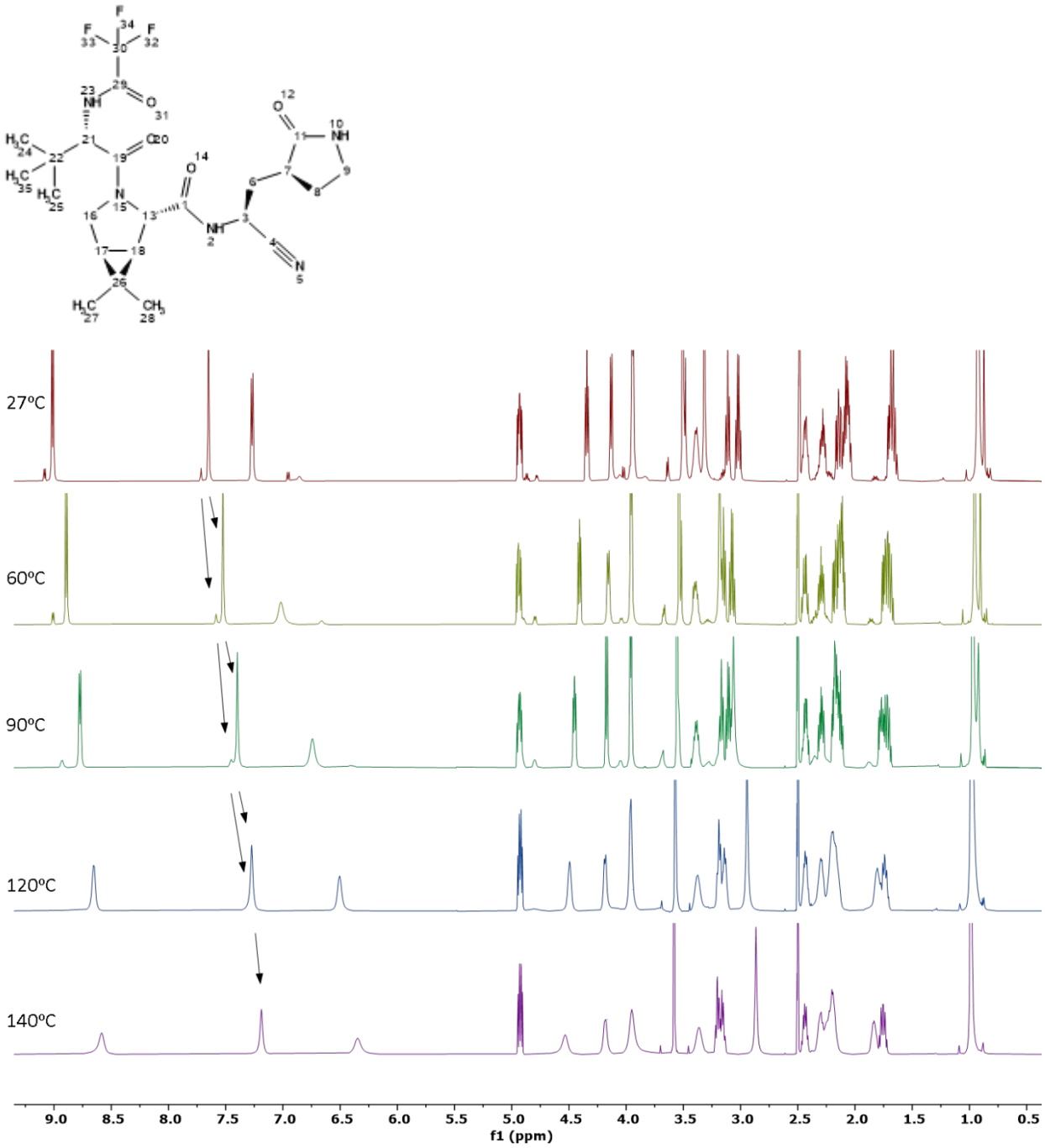

Figure S2. The ^{1}H-^{1}H NOESY spectra of compound **9** in dimethyl sulfoxide-d_6 at 60^{o}C. The resonances with restricted rotation are in chemical exchange and confirm the compound is a rotamer. The exchange peaks observed between the resonances with restricted rotation have the same sign (orange correlations) as the diagonal consistent with a transfer NOE. Actual through space NOEs in this experiment have the opposite sign as the diagonal and appear as blue correlations.

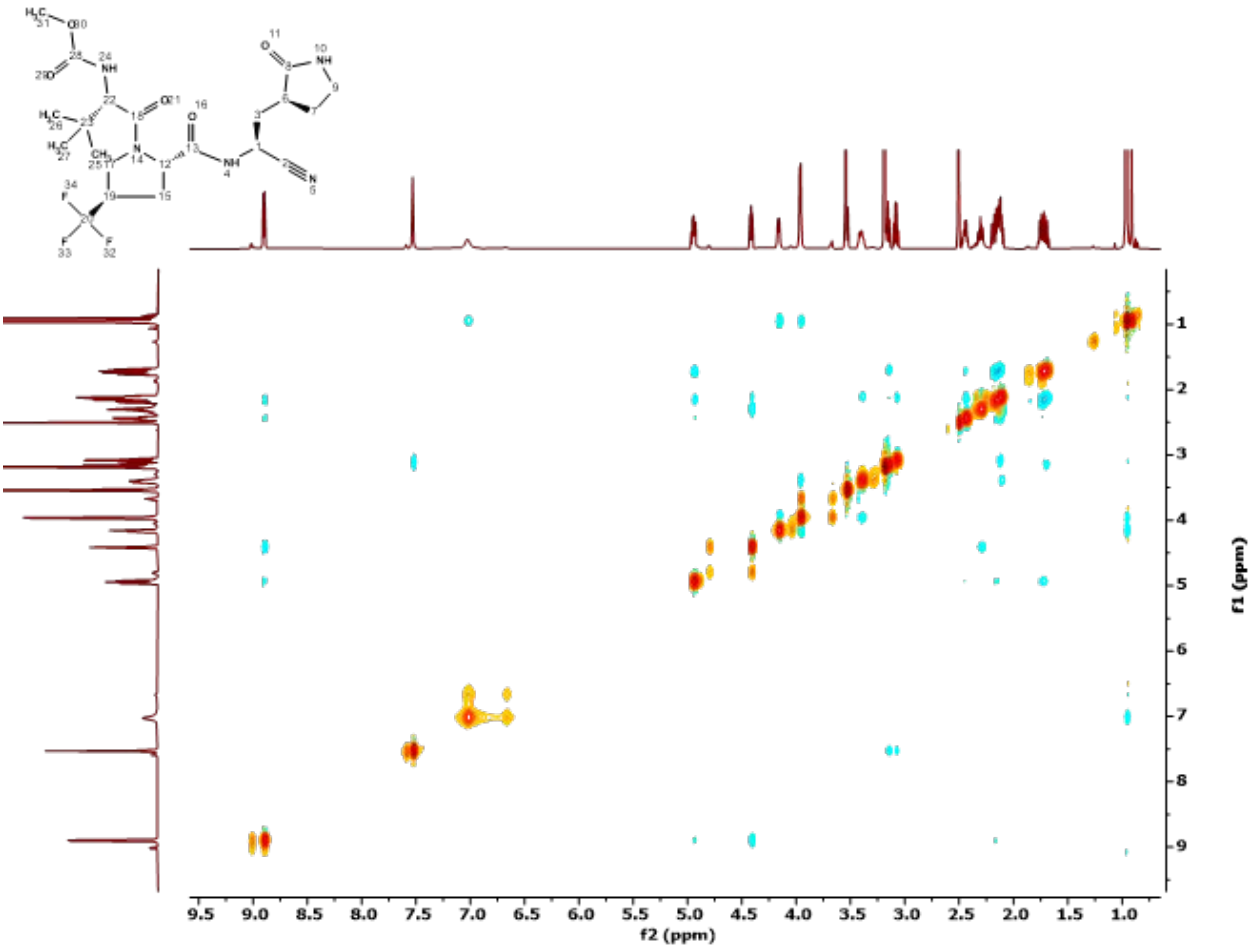

Figure S3. Metabolites derived from compound **9**

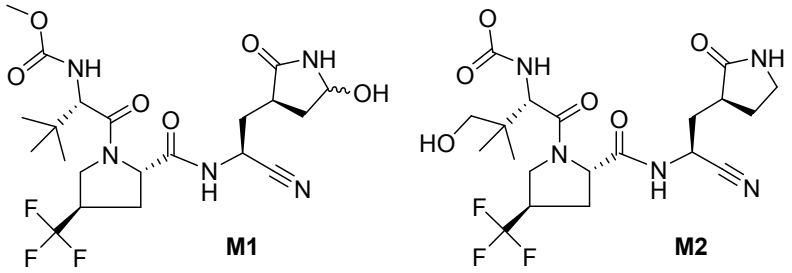

Figure S4. Mass Spectra for **9**. Top panel: MS^1; Lower Panel: MS^2 for *m/z* 490

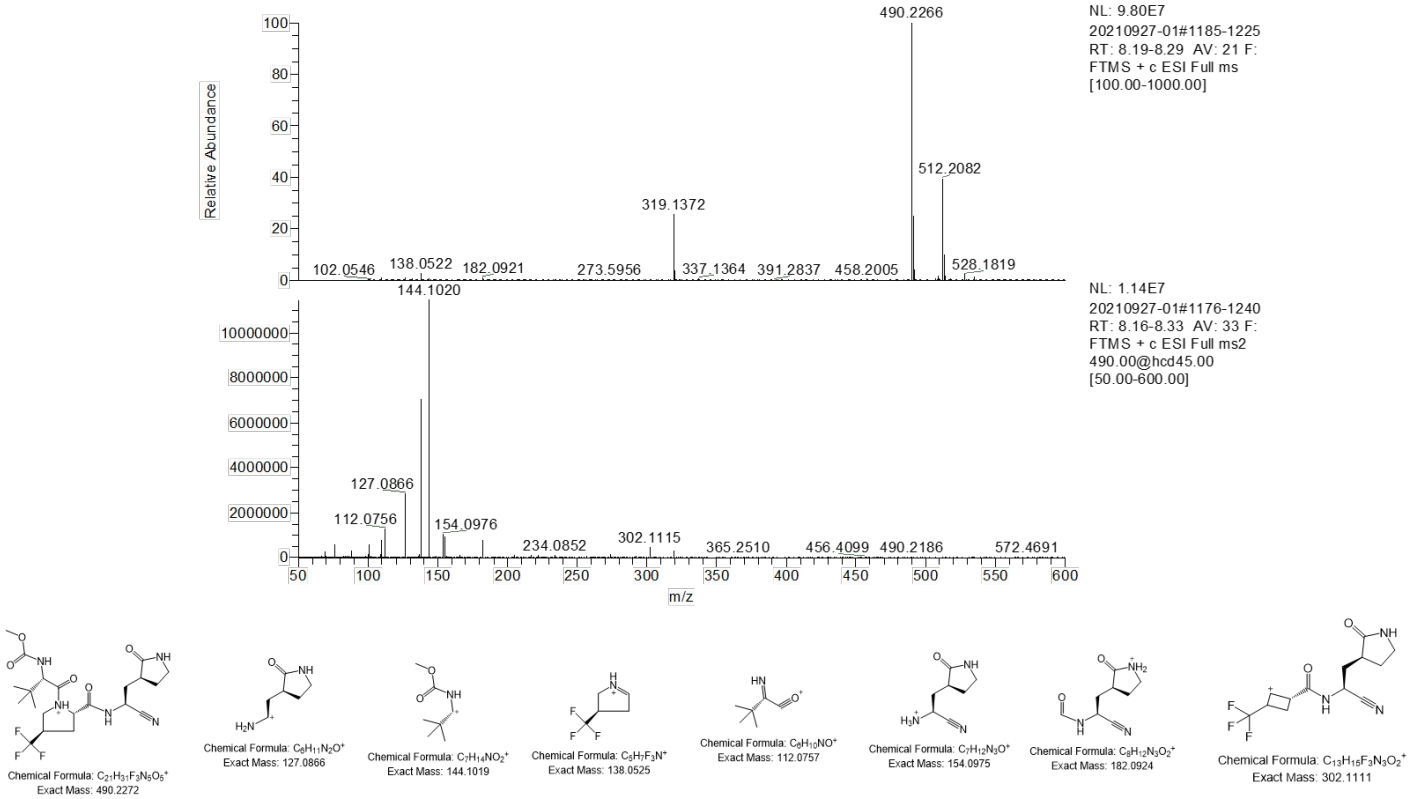

Figure S5. Mass Spectra for Metabolite M1 Observed in Human Liver Microsomal, Cytochrome P4503A, and Hepatocyte Incubations of **9**. Top panel: MS^1; Lower Panel: MS^2 for *m/z* 488 (Dehydrated Ion from *m/z* 506).

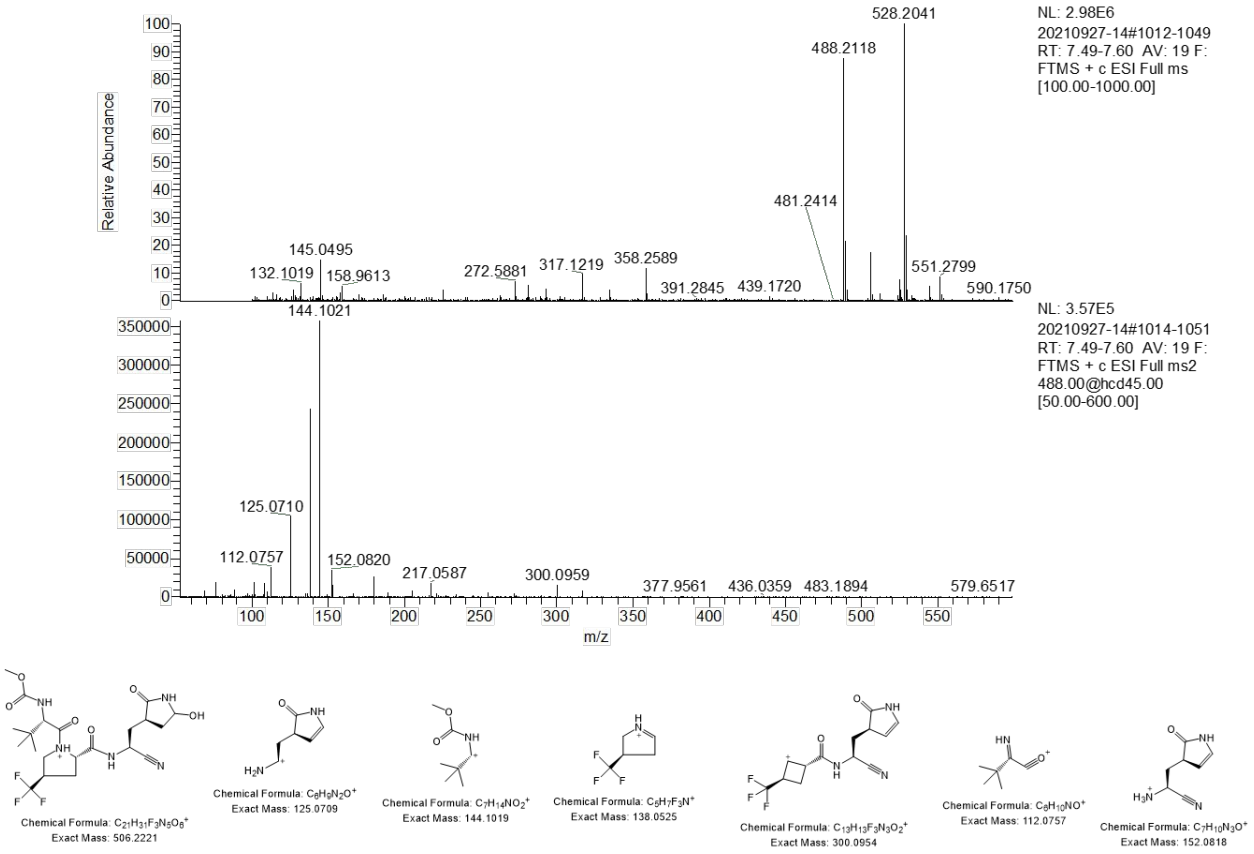

Figure S6. NMR Spectra for Biosynthesized Metabolite M1. A = 1H Spectrum. B = HSQC Spectrum showing the correlation between the 5-hydroxypyrrolidone proton and carbon at position 5.

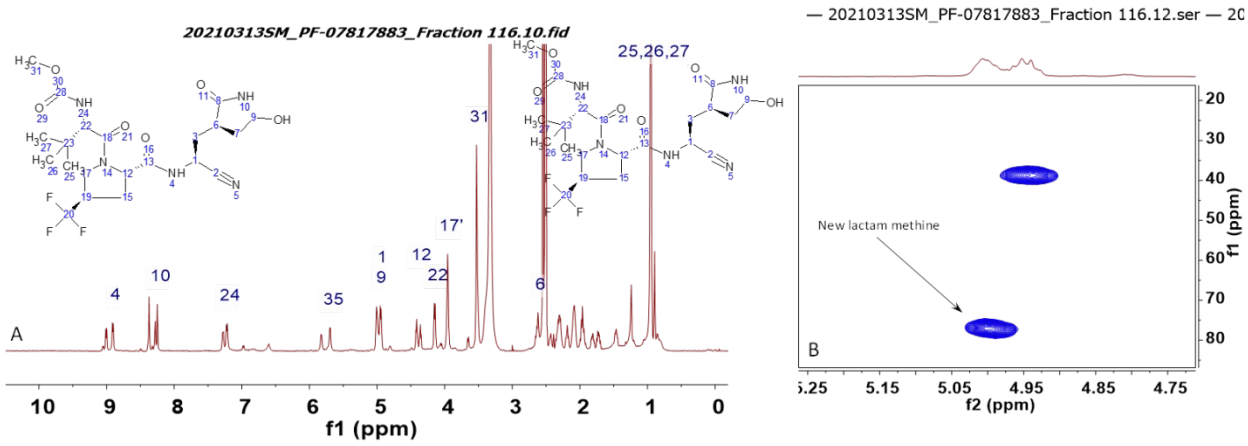

Figure S7. Mass Spectra for Metabolite M2 Observed in Human Liver Microsomal, Cytochrome P4503A, and Hepatocyte Incubations of **9**. Top panel: MS^1; Lower Panel: MS^2 for *m/z* 506.

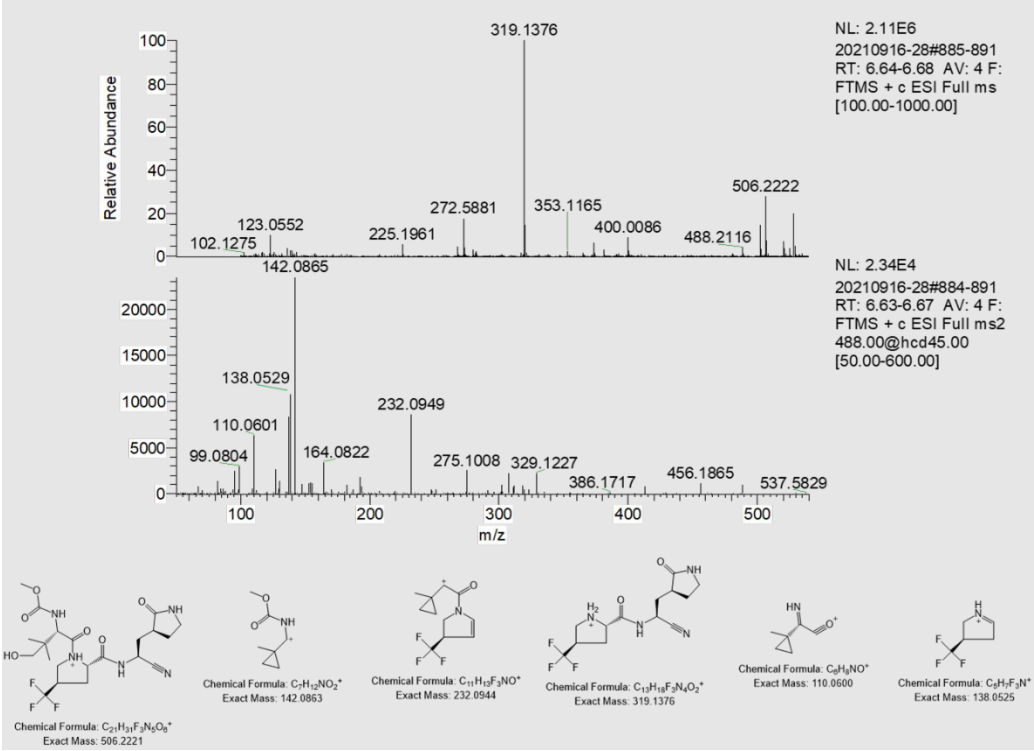

Figure S8. NMR Spectra for Biosynthesized Metabolite M2. A = 1H Spectrum. B and C = HMBC and HSQC Spectra demonstrating new coupling patterns on the t-butyl group.

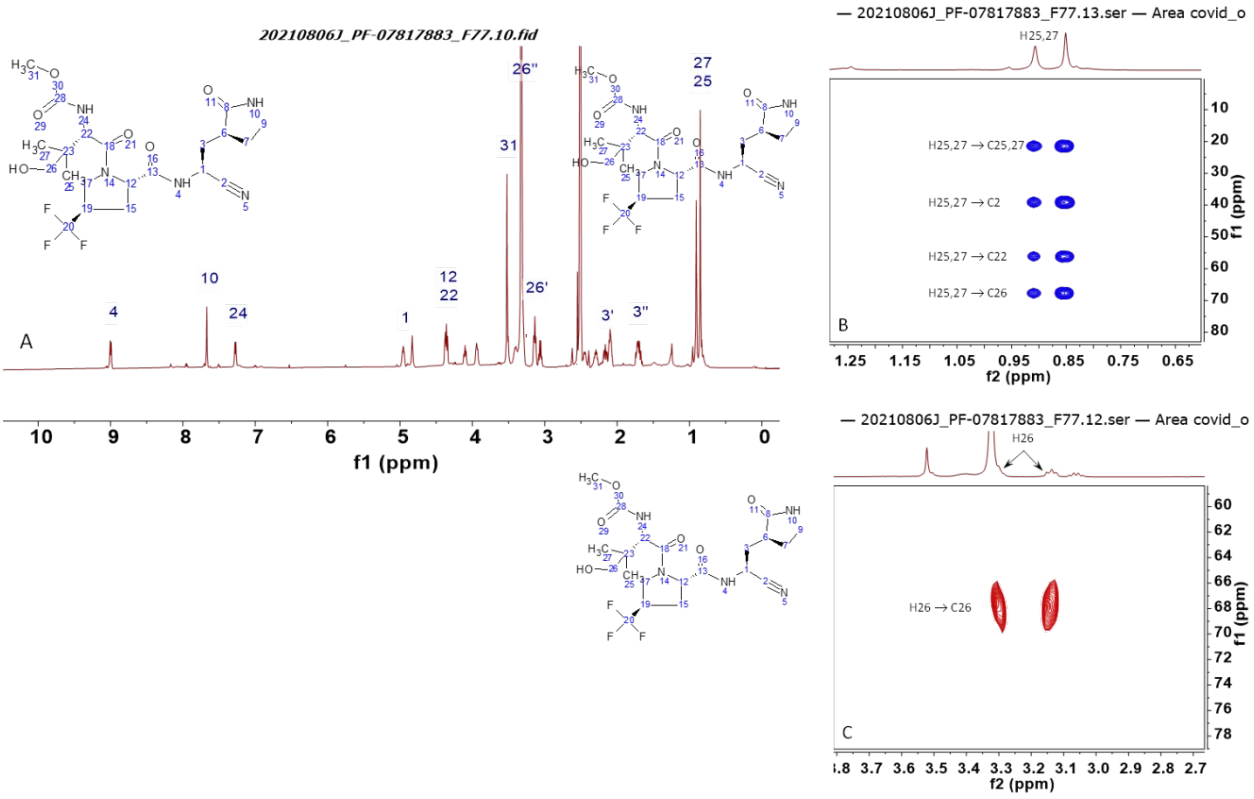

Recombinant SARS-CoV-2 M^{pro} Protease Production

Optimized synthetic genes coding for an *Escherichia coli* (*E. Coli*) expression M^{pro} protease enzyme from the SARS-CoV-2 virus (Wuhan-Hu-1 isolate; accession number MN908947) were designed and ordered from Genscript and IDT/BATJ. Two *E. Coli* expression constructs were prepared – SARS-CoV-2 M^{pro} protease (fully mature, authentic) and SARS-CoV-2 M^{pro}+G (SARS-CoV-2 M^{pro} protease with an additional Glycine at its N-terminus). The SARS-CoV-2 M^{pro} construct contains both N and C-terminal His tags. The N-terminal hexa-histidine tag followed with TEV cleavage-site (TTENLYFQ↓SGFRK, arrow indicates the cleavage site), was autocleaved by SARS-CoV-2 M^{pro} protease during expression to generate the mature N-terminus

At the C-terminus, the construct contained a GP hexa-histidine affinity tag, SGVTFQ↓GP, which is a modified PreScission cleavage site that was removed during the purification with PreScission protease. The SARS-CoV-2 M^{pro} +G construct contains an N-terminal hexa-histidine affinity tag with TEV cleavage-site (TTENLYFQ↓GSGFRK), which was removed during purification with TEV, leaving an extra glycine at the N-terminus E. Coli BL21(DE3) cells harboring the SARS-CoV-2 M^{pro} expression vector were grown in multiples of 500 ml of LB in 1 liter shake flasks for 5 hours post induction at 16 °C. *E. Coli* BL21(DE3) cells harboring the SARS-CoV-2 M^{pro} +G expression vector were grown in 6 L of Terrific Broth for 5 h post induction at 30 °C in a high density shake flask. Cell pellets were stored at -80 °C until purification.

Purification of SARS-CoV-2 M^{pro}

Cell pellets were resuspended and lysed in 50 mM tris(hydroxymethyl)aminomethane (Tris) pH 8, 250 mM NaCl, 10 mM imidazole, 0.25 mM TCEP (Buffer A) via microfluidization and clarified by centrifugation at 29,400 g for 60 min at 4 oC. Cleared lysate was added to Niprobond resin and incubated at 4 °C for 2 h. Ni-resin was loaded on a gravity column and after 15 column volumes washes in Buffer A, protein was eluted in 50 mM Tris pH 8, 250 mM NaCl, 200 mM imidazole, 0.25 mM TCEP. Eluted protein was incubated with TEV/Precision protease and dialyzed overnight. The dialyzed and tag-removed protein was filtered and run over 5 ml nickel column to remove the affinity tag, and the flow through was further purified loading on a Superdex-200 26/60 column equilibrated with 25 mM Tris pH 7.5, 150 mM NaCl, 1 mM EDTA, 1 mM DTT. Pooled fractions were concentrated to 7.10 mg/ml and aliquots were flash-frozen in liquid nitrogen and stored at -80 °C until crystallization.

Purification of SARS-CoV-2 M^{pro} +G

SARS-CoV-2 M^{pro}+G cells were lysed via microfluidization and clarified by centrifugation at 38,400 g for 60 min at 4 °C. Lysate was loaded onto a 5 ml HisTrap HP column in 50 mM Tris (pH 8.0), 500 mM NaCl, 20 mM imidazole, pH 8.0, 14 mM β-mercaptoethanol (β−ME) (buffer B). The column was washed with buffer B before eluting with 20 column volumes of 20-300 mM imidazole (0-75% buffer C: 50 mM Tris-HCl, pH 8.0, 500 mM NaCl, 400 mM imidazole, pH 8.0, 14 mM β−ME) and 10 column volumes 400 mM imidazole (100% buffer C). The nickel eluate was incubated with TEV protease to cleave the histidine tag and dialyzed overnight at 4 °C in 50 mM Tris-HCl (pH 8.0), 200 mM NaCl, 14 mM β−ME. The dialyzed and tag-removed protein was filtered and run over 5 ml nickel column to remove the affinity tag, and the flow through was loaded onto a 2 x 53 ml HiPrep Desalting column in 25 mM Tris-HCl (pH 8.0), 50 mM NaCl, 14 mM β−ME (Q buffer A). Pooled buffer-exchanged fractions were loaded onto a 10 ml Q column. Q flowthrough fractions containing the SARS-CoV2 M^{pro} +G enzyme were concentrated and loaded onto a Superdex 200 gel filtration column in 25 mM Tris (pH 7.5), 150 mM NaCl, 1 mM ethylenediaminetetraacetic acid (EDTA), and 1 mM DTT. Pooled fractions were concentrated to 11.77 mg/ml and filtered through a 0.2 μM filter. Aliquots were flash-frozen in liquid nitrogen and stored at -80 °C until crystallization.

Generation of Assay Ready Plates for Coronavirus M^{pro} and Mammalian Protease Assays

Test compounds were serially diluted by half-log in 100% DMSO 11 times with a top concentration of 3 mM or serially diluted by 2-fold in 100% DMSO 11 times with a top concentration of 0.1 mM. A volume of 300 nl of each dilution was spotted into a separate plate

ready for enzyme and substrate additions. The top dose of compound in the assay was 30 μM or 1 μM with the final DMSO concentration at 1%.

Crystallization and Structure Determination

Recombinant SARS-CoV-2 M^{pro} was purified as described previously.[25] Apo crystals of SARS-CoV-2 3CL protease were prepared with the mature and authentic SARS-CoV-2 3CL protease at 7.10 mg/mL. Protein was passed through a 0.45μM cellulose-acetate spin filter and set up for crystallization using an NT-8 crystallization robot (Formulatrix). Using MRC-2 crystallization plates, wells containing 50 μL of 20.0% w/v (20.0 μL of stock 50.0% w/v) PEG 3350 and 0.2 M (6.67 μL of stock 1.5 M) potassium sodium tartrate tetrahydrate were dispensed, and then sitting drops consisting of 0.3 μL protein were set up against 0.3 μL well buffer. Crystallization plates were incubated at 21^{o}C, and clusters of plates crystals measuring 0.2 x 0.2 x 0.05 mm grew in a few days. Crystals of PF-07817883 (**9**) bound to SARS-CoV-2 3CL protease were obtained by soaking PF-07817883 (**9**) into apo crystals of SARS-CoV-2 M^{pro}. Specifically, PF-07817883 (**9**) (100 mM stock in 100% DMSO) was mixed with well solution and added directly to the crystallization drop (approx. 1 mM final conc). These crystals were allowed to soak, undisturbed, at 30 ^{o}C for three days. Soaked crystals were then flash-cooled in liquid nitrogen after being passed through a cryo-protectant consisting of well buffer containing 20% ethylene glycol. X-ray diffraction data to 1.82 Å resolution were collected at IMCA-CAT 17-ID beamline of the Advanced Photon Source at Argonne National Labs and processed using autoPROC.[28] The structure of SARS-CoV-2 M^{pro} in complex with PF-07817883 was determined by difference Fourier using a previously determined in-house structure of SARS-CoV-2 M^{pro} protease as the starting model in the program DIMPLE in CCP4.[29] The ligand was fit automatically in AFITT.[30,

[31] The structure was refined iteratively by manual model building in Coot[32] followed by refinement in BUSTER[33] using the ligand parameter file generated in AFITT, with a final R and R_{free} factor of 21.61 % and 26.40 % respectively.

Table S1. Diffraction Data and Refinement Statistics for **9**

Data Statistics for X-ray diffraction data	
PDB entry ID	8V4U
Wavelength (Å)	1.0
Resolution	44.58 – 1.82
Space group	$P2_1$
Unit cell dimensions [Å]	a = 45.4, b = 54.1, c = 115.2
Unit cell dimensions [°]	$\alpha = \gamma = 90.0$, $\beta = 101.9$
Total number of reflections[a]	116082 (5774)
Unique reflections[a]	33627 (1682)
Multiplicity[a]	3.5 (3.4)
Completeness (%), spherical[a]	68.1 (14.2)
Completeness (%), ellipsoidal[a]	92.4 (53.6)
Mean $I/\sigma(I)$[a]	8.3 (1.5)
R_{merge}[b]	0.089 (0.759)
R_{pim}[c]	0.057 (0.485)
$CC_{1/2d}$	0.998 (0.618)
Refinement Statistics	
Reflections used	33627
Reflections used for R_{free}	1665
R_{cryst}[e]	0.216
R_{free}	0.264
Ramachandran Plot	

Favoured regions (%)	97.67
Allowed Regions (%)	2.16
Outlier regions (%)	0.17

[a] Numbers in parentheses refer to the highest resolution shell

[b] $R_{merge} = \sum_{hkl}\sum_{i=1}^{n} | I_i(hkl) - \bar{I}(hkl)| \; / \sum_{hkl}\sum_{i=1}^{n} I_i(hkl)$

[c] $R_{pim} = \sum_{hkl}\sqrt{1/(n-1)}\sum_{i=1}^{n} | I_i(hkl) - \bar{I}(hkl) / \sum_{hkl}\sum_{i=1}^{n} I_i(hkl)$ [34]

[d] $CC_{1/2}$ = xxx as defined by Karplus and Diederichs[35]

[e] $R_{cryst} = \sum_{hkl} | F_o(hkl) - F_c(hkl) | \sum_{hkl} | F_o(hkl) |$, where F_o and F_c are the observed and calculated structure factors, respectively.

R_{free} is the same as R_{cryst}, but for 5% of the data randomly omitted from refinement.[36]

Table S2. Biochemical Determination for Human Coronavirus M^{pro} Assays: Peptide Sequences and Reagent Parameters

Coronavirus Assay	Protease (nM)	Substrate (μM)	Peptide Sequence
SARS-CoV-2	15	25	Dabcyl-KTSAVLQ‖SGFRKME-Edans
SARS-CoV-1	25	25	Dabcyl-KTSAVL‖SGFRKM-Edans
MERS	100	25	Dabcyl-KTSAVL‖SGFRKM-Edans
HCoV-229E	50	12.5	Dabcyl- YGSTLQ‖GLRKM -Edans
NL63	50	12.5	Dabcyl- YNSTLQ‖SGLKKM -Edans
OC43	25	12.5	Dabcyl-KTSAVL‖SGFRKM-Edans

HKU1	12.5	12.5	Dabcyl-KTSAVLlSGFRKM-Edans

Compound **9** was tested at final concentrations up to 30 μM in1% DMSO and compared to the broad-spectrum antiviral compound GC376 (*52*) which produced 100% inhibition at 30 μM. Control wells (0% inhibition) contained 1% DMSO with substrate and protease and did not contain compound. The reaction was allowed to progress for 60 minutes at 23°C after which the plate was read on a Molecular Devices Spectramax M2e reader at an Ex/Em of 340 nm/490 nm.

Table S3. Mammalian Protease Panel: Peptide Sequences and Reagent Parameters

Protease/ class	Enzyme (nM)	Substrate (μM)	Substrate
Caspase2/ cysteine	10	5	Ac-LEHD-AMC
Cathepsin B/ cysteine	1.2	15	CBZ-Arg-Arg-AMC
Cathepsin D/ aspartyl	1.0	2	MCA-PLGL-Dap(Dnp)-AR-NH2
Cathepsin F/ cysteine	94	10	Z-Phe-Arg-AMC
Cathepsin K/ cysteine	0.25	2	Z-Phe-Arg-AMC
Cathepsin L/ cysteine	0.25	10	Z-Phe-Arg-AMC
Cathepsin S/ cysteine	1.5	10	Z-Phe-Arg-AMC
Cathepsin V/ cysteine	12	10	Z-Phe-Arg-AMC
Chymotrypsin/ serine	2.0	750	Suc-AAP-AMC
Elastase/ serine	0.6	10	MeOSuc-AAPV-AMC
HIV-1/ aspartyl	20	10	AnaSpec-SensoLyte
Thrombin a/ serine	0.01	10	H-D-CHA-Ala-Arg-AMC.2AcOH

The respective protease in assay buffer (50 mM Tris with 100 mM sodium chloride and Brij 35 at pH 8.0 except for cathepsin D pH 3.5 and HIV pH 5.5) was added to assay ready compound plates. The cathepsin L buffer was 400 mM sodium acetate pH 5.5 with 4 mM EDTA and 8 mM DTT. The enzymatic reaction was initiated with the addition of the indicated substrate in assay buffer and proceeded at room temperature for 2 h. Final concentrations of respective protease and substrate are shown in the table below. Final DMSO concentration was below 1%. Initial rates

were measured by following the fluorescence of the cleaved substrate using a Spectramax (Molecular Devices) fluorescence plate reader in the kinetic format.

Table S4. Selectivity of PF-07817883 against a panel of mammalian proteases and HIV1 protease.

Protease/ class	IC50 (uM)
Caspase2/ cysteine	>100
Cathepsin B/ cysteine	>100
Cathepsin D/ aspartyl	>100
Cathepsin F/ cysteine	20.6
Cathepsin K/ cysteine	0.0212
Cathepsin L/ cysteine	>100
Cathepsin S/ cysteine	0.0326
Cathepsin V/ cysteine	1.73
Chymotrypsin/ serine	>10
Elastase/ serine	>79.4
HIV-1/ aspartyl	>100
Thrombin a/ serine	>100

The inhibitory activity of PF-07817883 (**9**) was evaluated using FRET-based assay format at seven cysteine proteases (caspase 2, cathepsin B, cathepsin F, cathepsin K, cathepsin L, cathepsin S, cathepsin V); three serine proteases (chymotrypsin, elastase, thrombin a) and two aspartyl proteases (cathepsin D, HIV-1) each at the indicated protease and substrate concentrations. Data shown represent at least three independent experiments where there is a calculated value and at least two independent experiments where the value was greater than maximum tested concentration.

Data Analysis for Mammalian and Coronavirus Protease Panels

Percent inhibition values were calculated based on control wells containing DMSO only (0% inhibition) and wells containing a control compound (100% inhibition). IC_{50} values were generated based on a four-parameter logistic fit model

using ActivityBase software (IDBS). Percent activity values were calculated based on control wells containing no compound (100% activity), wells containing the broad-spectrum antiviral compound GC376 (0% activity) and wells containing an internal Pfizer control compound (0% activity). K_i values were fitted to the tight binding Morrison equation with fixed parameters for enzyme concentration, substrate concentration and the K_m parameter using ActivityBase software (IDBS) indicated below.

$$\text{TB Ki}: v_i = b + v0 * \left(1 - \frac{2*[I]}{E + [I] + Ki * \frac{[S] + Km}{Km} + \sqrt{\left(E + [I] + Ki * \frac{[S] + Km}{Km}\right)^2 - 4E[I]}}\right) = \text{function}(b, v0, Ki, E)$$

Assay	Enzyme (nM)	Substrate (μM)	K_m (μM)
229E	50	12.5	13.7
HKU1	12.5	12.5	18.3
MERS	100	25	21.3
NL63	50	12.5	13.5
OC43	25	12.5	18.1
SARS-CoV-1	25	25	39.3

Disposition Studies

Research was conducted on human tissue acquired from a third party that had been verified as compliant with Pfizer policies, including Institutional Review Board/Independent Ethics Committee approval. Human liver microsomes (HLM) (custom pool of 50 donors, male and female) were purchased from Sekisui XenoTech (Kansas City, KS) and human hepatocytes (HHEP) (custom pool of 13 donors, male and female) were purchased from BioIVT (Westbury, NY). β-Nicotinamide adenine dinucleotide phosphate, reduced form (NADPH), potassium dihydrogen phosphate (monobasic), dipotassium hydrogen phosphate (dibasic), magnesium

chloride, formic acid, and DMSO were obtained from Sigma Aldrich (St. Louis, MO). Acetonitrile (HPLC grade) was purchased from Fisher Scientific (Fair Lawn, NJ).

Metabolism of Compound 9 in Human Liver Microsomes and Human Hepatocytes. Microsomal incubations (0.2 mL) contained liver microsomes (2.0 mg protein/mL), Compound **9** (20 μM), 100 mM potassium phosphate buffer (pH 7.4), 3.3 mM $MgCl_2$, and 1.3 mM NADPH. Incubations were initiated with the addition of all components to the liver microsomes and were conducted at 37°C for 1 hour, followed by termination with three volumes of acetonitrile. Samples were subsequently centrifuged at 1800 × g for 5 minutes. The samples were then transferred to clean glass insert tubes and evaporated to dryness in a vacuum centrifuge (Genevac, SP Industries, Ipswich, UK). Finally, the residues were reconstituted in 75 μL of 20% acetonitrile in 1% formic acid. Human hepatocyte incubations (0.75×10^6 cells/mL Williams E media) containing 20 μM compound **9** were conducted at 37°C in an incubator maintained at 85% relative humidity. Aliquots (1 mL) were removed at 0 and 4 hours and quenched with five volumes of acetonitrile. Samples were subsequently centrifuged at 1800 × g for 5 minutes. The samples were then transferred to clean 15 mL glass tubes and evaporated to dryness using a vacuum centrifuge. The residues were reconstituted in 100 μL of 20% acetonitrile in 1% formic acid.

Ultrahigh Performance Liquid Chromatography (UHPLC)-High Resolution Mass Spectrometry for Metabolite Profiling. The UHPLC system consisted of a Thermo Vanquish quaternary pump, autoinjector maintained at 10°C, column heater maintained at 45°C, and diode array UV detector scanning from 200-400 nm (Thermo). Reconstituted extracts from in vitro and in vivo samples were injected (10-15 μL) on a Kinetex C18 XB column (2.1 × 100 mm; 2.6 μm;

Phenomenex, Torrance, CA). The mobile phase consisted of 0.1% formic acid in water (A) and acetonitrile (B) at a flow rate of 0.4 mL/minute. The initial condition of 5%B was held for 0.5 minutes followed by a linear gradient to 60%B at 11 minutes, a second linear gradient to 95%B at 13 minutes, held at that composition for 1 minute, followed by a 2 minute re-equilibration period at initial conditions. The eluent from the UHPLC was introduced into the source of an Orbitrap Elite high resolution mass spectrometer (Thermo, Waltham, MA) operated in the positive ion mode. The resolution was set at 30000. The source and capillary temperatures were set at 345°C and 275°C, respectively. Sheath, auxiliary, and sweep gases were set at 50, 10, and 2 (arbitrary units), and the source potential was set at 4 kV. Daughter spectra were generated using CID and HCD modes of fragmentation at collision energy settings of 35 and 45, respectively.

Biosynthesis of Metabolites M1 and M2 of Compound 9. Compound **9** (25 μM) was incubated with rabbit liver microsomes (2 mg/mL; Xenotech), $MgCl_2$ (3.3 mM), and NADPH (1.3 mM) in a volume of 40 mL potassium phosphate buffer (100 mM) at 37 °C for 90 minutes. To the incubation mixture was added acetonitrile (40 mL), the material was spun in a centrifuge (1800 × g; 5 minutes) and the supernatant was partially evaporated in a vacuum centrifuge (Genevac, SP Industries, Ipswich, UK). To this mixture was added formic acid (0.5 mL), acetonitrile (0.5 mL) and water to a volume of 50 mL. This mixture was spun in a centrifuge (40000 × g; 30 minutes) and the supernatant was applied to a Polaris C18 column (4.6 × 250 mm; 5μm; Neta Scientific, Hainesport, NJ) through a HPLC pump (Jasco, Easton, MD) at 0.8 mL/minute. After application, the column was moved to an Acquity HPLC-UV (Waters, Milford, MA) in line with a CTC Analytics (Zwingen, Switzerland) fraction collector and LTQ Velos (Thermo) mass spectrometer. The material was eluted with a gradient consisting of mobile phase A (0.1% formic acid in water)

and mobile phase B (acetonitrile) at 0.8 mL/minute. The gradient commenced at 5%B with a linear gradient to 20%B at 10 minutes, a second linear gradient to 60%B at 75 minutes, and a third linear gradient to 95%B at 90 minutes. This composition was held for 9 minutes followed by a 10-minute re-equilibration period to initial conditions. The eluent was passed through the UV detector, then a splitter that directed the flow to the fraction collector and mass spectrometer in an approximate 15:1 ratio. Fractions were collected every 20 seconds and those containing metabolites of interest were evaluated for purity by UHPLC-UV-MS (using the method described above) to facilitate fraction pooling. Pooled fractions were evaporated in the vacuum centrifuge and residues evaluated by quantitative NMR spectroscopy.

All samples were dissolved in 0.045 mL of DMSO-d_6 "100%" (Cambridge Isotope Laboratories, Andover, MA) and placed in a 1.7 mm NMR tube in a dry argon atmosphere. ^{1}H and ^{13}C spectra were referenced using residual DMSO-d6 (^{1}H δ=2.50 ppm relative to TMS, δ=0.00, ^{13}C δ=39.5 ppm relative to TMS, δ=0.00). NMR spectra for **9** and M1 were recorded on a Bruker Avance (Bruker BioSpin Corporation, Billerica, MA) controlled by Topspin V3.2 and equipped with a 1.7 mm TCI Cryo probe. NMR spectra for M2 was recorded on a Bruker Neo 600 MHz (Bruker BioSpin Corporation) controlled by Topspin V4.1 also equipped with a 1.7 mm TCI Cryo probe. 1D spectra were recorded using an approximate sweep width of 8400 Hz and a total recycle time of approximately 7 seconds. 2D data were recorded using the standard pulse sequences provided by Bruker. Post-acquisition data processing was performed with either Topspin V3.2 or MestReNova V14.1. Quantitation of NMR isolates were performed by external calibration against the ^{1}H NMR spectrum of a 5 mM benzoic acid standard using the quantitative functions within Topspin V3.2 or MestReNova.

Determination of the $CL_{int,app}$ for 9 in HLM. Protein concentration and incubation time were chosen to reflect linear reaction velocities determined in preliminary range finding experiments. Stock solutions were prepared in 90/10 acetonitrile/water at 100-times the final incubation concentration, resulting in a final acetonitrile concentration of 0.9% in the incubations. Compound **9** (0.5-184 μM) was incubated with HLM (0.1 mg/ml) in 100 mM potassium phosphate buffer (pH 7.4) supplemented with $MgCl_2$ (3.3 mM) and NAPDH (1.3 mM) for a final incubation volume of 200 μL. Incubations were conducted at 37 °C in triplicate and **9** was prepared from 3 separate weighings. After a 40 min incubation, a 100 μL aliquot of the incubation was quenched with 200 μL of acetonitrile containing internal standard indomethacin (50 ng/mL). Metabolites M1 (PF-07832809) and M2 (PF-07862061) standard curves were prepared in blank matrix at 1-3000 nM. Samples were vortexed, centrifuged (5 min, 2100 x g) and clean supernatant was diluted with an equal volume of water containing 0.2% formic acid. Samples were directly analyzed by liquid chromatography tandem mass spectrometry (LC-MS/MS). Integration and quantitation of metabolite and internal standard peak areas were performed using Analyst version 1.7 (Sciex, Framingham, MA) to derive the analyte to internal standard peak area ratios. Standard curves for the quantitation of metabolite concentrations were prepared from plots of area ratio versus concentration and analyzed using a linear regression with $1/x^2$ weighting. Formation rates (v) were calculated by dividing the measured metabolite concentration by incubation time and protein concentration of the incubation. The rate of metabolite formation was not saturated within the substrate concentration range tested, so the slope of the initial linear portion of the velocity versus substrate concentration data was calculated (by linear regression) as a surrogate for V_{max}/K_m ($CL_{int,app}$). The slopes were summed for metabolites M1 and M2 to calculate the $CL_{int,app}$ for **9**.

Pharmacokinetics Studies. All activities involving animals were conducted in accordance with federal, state, local and institutional guidelines governing the use of laboratory animals in research in AAALAC accredited facilities and were reviewed and approved by Pfizer's or Bioduro's Institutional Animal Care and Use Committee.

Rat Pharmacokinetics. Rat pharmacokinetics studies were done at Pfizer (Groton, CT) or BioDuro Pharmaceutical Product Development Inc. (Shanghai, PRC); Jugular vein-cannulated male Wistar-Hannover rats were purchased from Charles River Laboratories, Inc. (Wilmington, MA) or Vital River (Beijing, PRC) and were typically 7-10 weeks of age at the time of dosing. During the pharmacokinetic studies, all animals were housed individually. Access to food and water was provided ad libitum (i.e., animals were dosed in the fed state). Compounds **5, 6, 9**, and **12** were administered iv via the tail vein ($n = 2 - 3$) dosed as a solution (1 mg/kg, 1 mL/kg) or via oral gavage ($n = 2 - 3$) as a solution or suspension (10 mg/kg, 10 mL/kg). Doses of compound **5** were prepared immediately before dosing. Serial blood samples were collected via the jugular vein cannula at predetermined timepoints after dosing. Animals were monitored for pain or distress throughout the study, with at least daily monitoring during normal husbandry prior to study start. At the study's completion, animals were euthanized by overdose of inhaled anesthesia followed by exsanguination. Blood samples were collected into tubes containing K_2EDTA and stored on ice until centrifugation to obtain plasma, which was stored frozen at -20 °C or lower.

Monkey Pharmacokinetics. All procedures performed on cynomolgus monkeys were in accordance with regulations and established guidelines and were reviewed and approved by an

Institutional Animal Care and Use Committee through an ethical review process. Monkey studies were conducted at Pfizer (Groton, CT). Male cynomolgus monkeys were purchased from Covance (Princeton, NJ), Charles River Laboratories, Inc. (Wilmington, MA), or Envigo Global Services (Indianapolis, IN); subjects 3-8 years of age were used in pharmacokinetic studies. For each study (*n=2–3*), compound 9 was dosed intravenously via either the saphenous vein or cephalic vein (typically 1 mg/kg and 1– 2 mL/kg) or via oral gavage (typically 5–10 mg/kg, 5 mL/kg). Animals were monitored for pain or distress throughout the study followed by at least daily monitoring while off study. The iv-dosing vehicle was optimized such that the compounds were in solution and stable for at least 24 h. In cases where overnight formulation stability could not be achieved, doses of test compound were prepared immediately before dosing. The composition of each dosing vehicle is provided in table 4 legend. Serial blood samples were collected via the femoral vein at predefined time points post-dose. Blood samples were collected into K_3EDTA treated collection tubes and were stored on wet ice prior to being centrifuged to obtain plasma, which was stored frozen at -20 °C or lower.

Mouse Pharmacokinetics. All procedures performed on BALB/c mice were in accordance with regulations and established guidelines and were reviewed and approved by an Institutional Animal Care and Use Committee through an ethical review process. Mice were weighed once before initiation of dosing and once pre-dose on Day 1. A total of 9 BALB/c mice (Charles River, 8-week-old female, n=3 mice/group) were divided into 3 groups: 100, 300, or 500 mg/kg BID for oral administration of PF-07817883. An ASD of PF-07817883 was solubilized in 1% (w/v) soluplus and 0.5% (w/v) methylcellulose A4M in deionized water by geometric dilution and was administered twice daily (BID) for 3 days. Blood samples were collected at 1, 3, 6, and 12 hours

after the first daily dose on Day 3. After final blood collection, mice were euthanized by CO_2 inhalation followed by bilateral thoracotomy Blood samples were collected into tubes containing K_2EDTA and stored on ice until centrifugation to obtain plasma, which was stored frozen at -20 °C or lower. Samples were quantified via LC-MS/MS against a standard curve as described in the LC-MS/MS analysis methods.

LC-MS/MS Analysis of In Vitro Samples. LC-MS/MS analysis was performed using a Sciex Triple Quad 5500 or 6500 mass spectrometer (Sciex, Framingham, MA), equipped with electrospray sources and Agilent 1290 binary pump (Santa Clara, CA). Aqueous mobile phase (A) was comprised of 0.1% formic acid in water and organic mobile phase (B) consisted of 0.1% formic acid in acetonitrile. Samples (10 µl) from various in vitro incubations were injected onto a Kinetex XB-C18 (2.1 x 50 mm, 1.7 µm) (Phenomenex, Torrance, CA) column at room temperature with a flow rate of 0.5 ml/min. The gradient program typically began with 10% initial mobile phase B held for 0.4 min, followed by a linear gradient to 60% B over 2.6 min, then to 95% over 0.4 min, held at 95% B for 0.6 min followed by re-equilibration to initial conditions for at least 0.4 min. The mass spectrometer was operated in multiple reaction monitoring mode, in positive and negative detection mode (polarity switching), with the following mass transitions (Q1/Q3) and collision energies (CEs):

Compound	Q1	Q3	CE
1	500	319	22
9	490	319	21
PF-07832809 (M1)	488 (optimized Q1 mass representing loss of water in source)	317	18

PF-07862061 (M2)	506	319	15
Indomethacin (Internal Standard)	358	139	27

LC-MS/MS Analysis of Plasma and Urine Samples. Plasma and urine samples were processed using protein precipitation with 100% acetonitrile containing a cocktail of internal standards followed by quantitation against a standard curve (0.5-50,000 ng/mL) prepared in blank control plasma. Urine samples were initially diluted 10-fold in control plasma and treated as plasma going forward. Quantitation of analyte in plasma and urine samples was done using a Sciex Triple Quad 5500 or 6500+ mass spectrometer (Sciex, Framingham, MA), equipped with an electrospray source and a Waters Acquity UPLC I Class PLUS System (Milford MA). Standards, prepared in blank control plasma were extracted in the same manner as the in-life samples. Separation was accomplished using a Waters Acquity UPLC HSS T3 column (1.8 µm, 2.1 × 50 mm) or a Waters Acquity UPLC BEH column (1.7 µm, 2.1 × 50 mm) maintained at either room temperature or 60 °C. The mobile phase (2 solvents gradient) was optimized to achieve good separation between the analytes. Typically, solvent A is water containing 0.5% formic acid, and solvent B is acetonitrile containing 0.5% formic acid. The gradient had a flow of 0.6 mL/min and generally began at 5-10% B until 0.1 min, followed by an increase to 90-99% B at 2.1 min, then decreased back to 5-10% B at 2.6 min, maintaining initial conditions from 2.6-3 min. MS/MS methods for different analytes analyzed in plasma and urine samples are presented in Table 1. Analyst 1.7 software was used for peak integration and standard curve regression.

Compound	Q1	Q3	DP	CE	Retention Time (min)	Internal Standard	Injection Volume (uL)

5	506.3	335.2	101	21	1.76	Terfenadine	10 (Sciex 5500)
6	590.3	291.2	60	25	1.27	Indomethacin	4
9	490.3	319.2	60	25	1.05	Verapamil	4
12	490.2	333.1	60	25	1.06	Verapamil	1.5
Indomethacin (150 ng/mL)	358.3	139.2	46	26	-	-	-
Terfenadine (30 ng/mL)	472.1	436	80	30	-	-	-
Verapamil (2.5 ng/mL)	455.2	165.4	60	45	-	-	-

Pharmacokinetic Analysis. Pharmacokinetic parameters were calculated using noncompartmental analysis (Watson v.7.5, Thermo Scientific). The area under the plasma concentration-time curve from $t = 0$ to infinity ($AUC_{0-\infty}$) was estimated using the linear trapezoidal rule. In some instances, pharmacokinetic calculations were generated using the linear log-linear trapezoidal rule and C_0 was calculated using the equation:

$$C_0 = \frac{Dose_{iv}}{V_b \times BPR}$$

where V_b is the blood volume (rat, 69.0 mL/kg; monkey, 62.3 mL/kg) and BPR is the blood to plasma ratio. Plasma clearance (CL_p) was calculated as:

$$CL_p = \frac{Dose_{iv}}{AUC_{0-\infty}}$$

The terminal rate constant (k_{el}) was calculated by linear regression of the terminal phase of the log-linear concentration-time curve and the terminal elimination $t_{1/2}$ was calculated as:

$$t_{\frac{1}{2}} = \frac{0.693}{k_{el}}$$

Apparent steady state distribution volume (Vd_{ss}) was determined by clearance multiplied by mean residence time. Oral bioavailability (F) was defined as:

$$F = \frac{AUC_{po} \times Dose_{iv}}{AUC_{iv} \times Dose_{po}}$$

The fraction of the oral dose absorbed (F_a x F_g) was estimated using the equation:

$$F_a \times F_g = \frac{F}{1 - \frac{CL_{blood}}{Q}}$$

A hepatic blood flow (Q) of 70 mL/min/kg and 44 mL/min/kg was used for rats and monkeys, respectively. Blood clearance (CL_{blood}) was calculated by dividing CL_p by the blood-to-plasma ratio (ranging from 0.6–0.8) for the compounds in the respective preclinical species.

Table S5. Induction of CYP3A4 mRNA and enzyme activity by compound **9**

Compound **9**		
	CYP3A4 mRNA[a]	CYP3A4 Activity[a]

Donor	Linear Slope ± SE (μM)	R^2 value	Data points applied	Test Concentration Range μM)	EC_{50} ± SE (μM)	Ind_{max} ± SE	γ ± SE
BXM	0.0341 ± 0.0013	0.977	11	0-200	102 ± 28	2.83 ± 0.28	1.46 ± 0.32
BNA	0.0450 ± 0.0015	0.982	12	0-300	151 ± 63	3.08 ± 0.64	1.95 ± 0.70
FOS	0.0192 ± 0.0009	0.957	12	0-300	ND	ND	ND

Three individual donor preparations of cryopreserved human hepatocytes were used to study CYP3A4 induction by **9**. Linear slope, EC_{50}, Ind_{max} and γ ± standard error (SE) for induction of CYP3A4 mRNA and midazolam-1′-hydroxylase activity by **9** in three lots of human hepatocytes. [a]fold induction of CYP3A4 mRNA or enzyme activity (midazolam-1′-hydroxylase) in human hepatocytes expressed as pmol/min/million cells. Linear slope is representative of E_{max}/EC_{50}. For γ calculations, CYP3A4 activity data was fit using a four-parameter sigmoidal model for BNA and BXM human hepatocyte lots. ND: not determined because of a lack of induction of CYP3A4 activity.

Table S6. Reversible and time-dependent inhibition of CYP Enzymes by compound **9**

Isoform	Enzyme Reaction (Probe Substrate)	Mean IC_{50}[a] (μM) with no pre-incubation	Inhibition at 100 μM (%)	Mean IC_{50}[a] (μM) with 30 minute pre-incubation	Inhibition at 100 μM (%)
CYP1A2	Phenacetin O-deethylation (Phenacetin, 30.0 μM)	>100	16.2	>100	8.89
CYP2B6	Bupropion hydroxylation (Bupropion, 89.6 μM)	>100	15.3	>100	19.8
CYP2C8	Amodiaquine N-deethylation (Amodiaquine, 1.66 μM)	>100	4.26	>100	1.19
CYP2C9	Diclofenac 4'-hydroxylation (Diclofenac, 6.45 μM)	>100	2.22	>100	9.47

CYP2C19	S-Mephenytoin 4′-hydroxylation (S Mephenytoin, 39.3 μM)	>100	24.2	>100	8.47
CYP2D6	Dextromethorphan O-demethylation (Dextromethorphan, 1.81 μM)	>100	2.44	>100	5.56
CYP3A4/5	Midazolam 1′-hydroxylation (Midazolam, 2.09 μM)	>100	19.4	>100	36.0
CYP3A4/5	Testosterone 6□-hydroxylation (Testosterone, 38.6 μM)	>100	18.1	>100	29.1
CYP3A4/5	Nifedipine oxidation (Nifedipine, 4.00 μM)	>100	17.6	>100	33.2

Reversible and time-dependent inhibition of CYPs by compound **9** was studied using human liver microsomes with incubations testing compound **9** concentrations from 0.01–100 μM. Probe CYP substrate concentrations were near enzyme affinity or Michaelis constant (K_m) values.[17] Time-dependent inhibition was defined as an IC_{50} shift of >1.5 fold or a ≥20% decrease in T_0-T_{30} activity at any test concentration. [a]total IC_{50}

Table S7. Reversible inhibition of major human intestinal, hepatobiliary and renal transporters by **9**.

Transporter	Test System	Probe Substrate	Estimated IC_{50} (μM)	% Inhibition at highest concentration (300 μM)
BCRP	HEK293 Vesicles	Rosuvastatin (0.2 μM)	>300	4.2
MATE1	HEK293 Cells	[^{14}C]-Metformin (20 μM)	>300	33.5
MATE2K	HEK293 Cells	[^{14}C]-Metformin (20 μM)	>300	22.6
MDR1	HEK293 Vesicles	N-methyl quinidine (0.2 μM)	274.9	54.9
OAT1	HEK293 Cells	[^{3}H]-Para-aminohippuric acid (0.5 μM)	>300	10.1
OAT3	HEK293 Cells	[3H]-Estrone-3-sulfate (0.1 μM)	>300	17.0

OATP1B1	HEK293 Cells	Rosuvastatin (0.3 µM)	294.5	49.3
OATP1B3	HEK293 Cells	Rosuvastatin (0.3 µM)	>300	1.0
OCT1	HEK293 Cells	[^{14}C]-Metformin (20 µM)	>300	47.0
OCT2	HEK293 Cells	[^{14}C]-Metformin (20 µM)	>300	18.7

Probe substrate concentrations selected << K_m for tested transporter. Compound **9** test concentrations ranged from 0.018-300 µM. HEK: human embryonic kidney. BCRP: Breast cancer resistance protein; MATE: multidrug and toxin extrusion protein; MDR: Multidrug resistance protein; OAT: organic anion transporter; OATP: organic anion transporting polypeptide; OCT: organic cation transporter.

Table S8. Data from Tables 1&2 SARS-CoV-2 M^{pro} K_i

Compound	End point	Result count	Result operator	GeoMean (nM)	Lower CI G	Upper CI G
1	Ki	6	=	3.11	1.47	6.6
2	Ki	3	=	5.49	3.86	7.8
3	Ki	5	=	1.12	0.66	1.92
4	Ki	6	=	0.70	0.16	3.11
5	Ki	6	=	0.63	0.22	1.79
6	Ki	5	=	2.83	1.42	5.61
7	Ki	4	=	3.88	2.7	5.58
8	Ki	3	=	4.46	1.23	16.23
9	Ki	5	=	2.48	1.21	5.06
10	Ki	5	=	0.17	0.09	0.33
11	Ki	4	=	13.27	5.96	29.57
12	Ki	6	=	1.13	0.76	1.67

Table S9. Data from Figure 5A Compound **9** Antiviral Activity Against Related Human Coronaviruses

Virus	Result Count	Result Operator	K_i GeoMean (nM)	Lower CI	Upper CI
229E	6	=	216	201	234
HKU1	6	=	50.7	30.2	85.2

MERS	6	=	597	388	919
NL63	6	=	1067	999	1140
OC43	6	=	38.1	30.7	47.2
SARS-Cov-1	6	=	9.78	6.56	14.6
SARS-Cov-2	5	=	2.48	1.21	5.06

Table S10. Data from Figure 5B Compound **9** Antiviral Activity Against Related Human Coronaviruses

Virus Strain	Host Cell	Compound **9** (µM; GeoMean)				Compound **9** + P-gp inhibitor (µM; GeoMean)			
		EC_{50} (95% CI)	**EC_{90} (95% CI)**	**CC_{50} (95% CI)**	**TI[a]**	**EC_{50} (95% CI)**	**EC_{90} (95% CI)**	**CC_{50} (95% CI)**	**TI[a]**
SARS-CoV-1[b]	VeroE6	22.1 (18.1-27.1)	46.0 (37.6-56.3)	>100 (ND)	4.62	0.157 (0.0933-0.266)	0.331 (0.194-0.564)	>100 (ND)	>797
HCoV-229E[b]	MRC-5	0.844 (0.498-1.43)	1.85 (1.19-2.87)	>100 (ND)	>127	--	--	--	--
MERS-CoV[b]	Vero81	12.1 (10.9 -13.5)	26.3 (24.1-28.6)	>100 (ND)	>8.35	0.158 (0.115-0.217)	0.329 (0.239-0.452)	>100 (ND)	>705

a. Individual TI values were calculated by dividing CC_{50} by EC_{50} values for the individual experiments then determining the average TI value.
b. The EC_{50}, EC_{90}, and CC_{50} values were determined from N = 4 to 10 (for both **9** alone and **9** + P--gp inhibitor CP-100356).

Table S11. Antiviral activity of **9** and remdesivir against SARS-CoV-2 strains of VOC alpha, beta and gamma in VeroE6-Pgp-KO cells

SARS-CoV-2	Drug	N	Geo Mean EC_{50} (nM) (Range)	N	Geo Mean EC_{90} (nM) (Range)
USA-WA1	Remdesivir	4	29.7 (18.5 – 75.4)		139.4 (58.7 – 569.8)
	9	4	31.3	4	266.9

			(15.48 – 67.93)		(73.6 – 494.0)
α Variant	Remdesivir	5	9.6 (5.5 – 32.9)	5	68.4 (33.1 – 138.8)
	9	3	40.8 (13.4 – 133.9)	3	306.9 (80.8 – 482.6)
β Variant	Remdesivir	6	11.8 (6.6 – 17.1)	6	109.6 (39.7 – 459.8)
	9	2	175.6* (115.7 – 235.5)	2	782.8* (771.5 – 794.0)
γ Variant	Remdesivir	6	7.0 1.6 – 18.0	6	36.4 (10.0 – 132.9)
	9	3	111.8 (66.6 – 148.5)	3	639.1 (466.6 – 836.7)

*Average

References

1. Zhu, Z.; Lian, X.; Su, X.; Wu, W.; Marraro, G. A.; Zeng, Y., From SARS and MERS to COVID-19: a brief summary and comparison of severe acute respiratory infections caused by three highly pathogenic human coronaviruses. *Respir Res* **2020,** *21* (1), 224.
2. WHO COVID-10 Dashboard. https://covid19.who.int/ (accessed October 31, 2023).
3. Toussi, S. S.; Hammond, J. L.; Gerstenberger, B. S.; Anderson, A. S., Therapeutics for COVID-19. *Nat Microbiol* **2023,** *8* (5), 771-786.
4. Taylor, P. C.; Adams, A. C.; Hufford, M. M.; de la Torre, I.; Winthrop, K.; Gottlieb, R. L., Neutralizing monoclonal antibodies for treatment of COVID-19. *Nat Rev Immunol* **2021,** *21* (6), 382-393.
5. Cox, M.; Peacock, T. P.; Harvey, W. T.; Hughes, J.; Wright, D. W.; Consortium, C.-G. U.; Willett, B. J.; Thomson, E.; Gupta, R. K.; Peacock, S. J.; Robertson, D. L.; Carabelli, A. M., SARS-CoV-2 variant evasion of monoclonal antibodies based on in vitro studies. *Nat Rev Microbiol* **2023,** *21* (2), 112-124.
6. Hammond, J.; Leister-Tebbe, H.; Gardner, A.; Abreu, P.; Bao, W.; Wisemandle, W.; Baniecki, M.; Hendrick, V. M.; Damle, B.; Simon-Campos, A.; Pypstra, R.; Rusnak, J. M.; Investigators, E.-H., Oral Nirmatrelvir for High-Risk, Nonhospitalized Adults with Covid-19. *N. Eng. J. Med.* **2022,** *386* (15), 1397-1408.
7. Tian, F.; Feng, Q.; Chen, Z., Efficacy and Safety of Molnupiravir Treatment for COVID-19: A Systematic Review and Meta-Analysis of Randomized Controlled Trials. *Int J Antimicrob Agents* **2023,** *62* (2), 106870.
8. Beigel, J. H.; Tomashek, K. M.; Dodd, L. E.; Mehta, A. K.; Zingman, B. S.; Kalil, A. C.; Hohmann, E.; Chu, H. Y.; Luetkemeyer, A.; Kline, S.; Lopez de Castilla, D.; Finberg, R. W.; Dierberg, K.; Tapson, V.; Hsieh, L.; Patterson, T. F.; Paredes, R.; Sweeney, D. A.; Short, W. R.; Touloumi, G.; Lye, D. C.; Ohmagari, N.; Oh, M. D.; Ruiz-Palacios, G. M.; Benfield, T.; Fatkenheuer, G.; Kortepeter, M. G.; Atmar, R. L.; Creech, C. B.; Lundgren, J.; Babiker, A. G.; Pett, S.; Neaton, J. D.; Burgess, T. H.; Bonnett, T.; Green, M.; Makowski, M.; Osinusi, A.; Nayak, S.; Lane, H. C.; Members, A.-S. G., Remdesivir for the Treatment of Covid-19 - Final Report. *N. Eng. J. Med.* **2020,** *383* (19), 1813-1826.

9. Jiang, X.; Su, H.; Shang, W.; Zhou, F.; Zhang, Y.; Zhao, W.; Zhang, Q.; Xie, H.; Jiang, L.; Nie, T.; Yang, F.; Xiong, M.; Huang, X.; Li, M.; Chen, P.; Peng, S.; Xiao, G.; Jiang, H.; Tang, R.; Zhang, L.; Shen, J.; Xu, Y., Structure-based development and preclinical evaluation of the SARS-CoV-2 3C-like protease inhibitor simnotrelvir. *Nat Commun* **2023,** *14* (1), 6463.
10. Mackman, R. L.; Kalla, R. V.; Babusis, D.; Pitts, J.; Barrett, K. T.; Chun, K.; Du Pont, V.; Rodriguez, L.; Moshiri, J.; Xu, Y.; Lee, M.; Lee, G.; Bleier, B.; Nguyen, A. Q.; O'Keefe, B. M.; Ambrosi, A.; Cook, M.; Yu, J.; Dempah, K. E.; Bunyan, E.; Riola, N. C.; Lu, X.; Liu, R.; Davie, A.; Hsiang, T. Y.; Dearing, J.; Vermillion, M.; Gale, M., Jr.; Niedziela-Majka, A.; Feng, J. Y.; Hedskog, C.; Bilello, J. P.; Subramanian, R.; Cihlar, T., Discovery of GS-5245 (Obeldesivir), an Oral Prodrug of Nucleoside GS-441524 That Exhibits Antiviral Efficacy in SARS-CoV-2-Infected African Green Monkeys. *J Med Chem* **2023,** *66* (17), 11701-11717.
11. Mukae, H.; Yotsuyanagi, H.; Ohmagari, N.; Doi, Y.; Sakaguchi, H.; Sonoyama, T.; Ichihashi, G.; Sanaki, T.; Baba, K.; Tsuge, Y.; Uehara, T., Efficacy and Safety of Ensitrelvir in Patients With Mild-to-Moderate Coronavirus Disease 2019: The Phase 2b Part of a Randomized, Placebo-Controlled, Phase 2/3 Study. *Clin Infect Dis* **2023,** *76* (8), 1403-1411.
12. Renjifo, B.; van Wyk, J.; Salem, A. H.; Bow, D.; Ng, J.; Norton, M., Pharmacokinetic enhancement in HIV antiretroviral therapy: a comparison of ritonavir and cobicistat. *AIDS Rev* **2015,** *17* (1), 37-46.
13. Eng, H.; Dantonio, A. L.; Kadar, E. P.; Obach, R. S.; Di, L.; Lin, J.; Patel, N. C.; Boras, B.; Walker, G. S.; Novak, J. J.; Kimoto, E.; Singh, R. S. P.; Kalgutkar, A. S., Disposition of Nirmatrelvir, an Orally Bioavailable Inhibitor of SARS-CoV-2 3C-Like Protease, across Animals and Humans. *Drug Metab Dispos* **2022,** *50* (5), 576-590.
14. Singh, R. S. P.; Toussi, S. S.; Hackman, F.; Chan, P. L.; Rao, R.; Allen, R.; Van Eyck, L.; Pawlak, S.; Kadar, E. P.; Clark, F.; Shi, H.; Anderson, A. S.; Binks, M.; Menon, S.; Nucci, G.; Bergman, A., Innovative Randomized Phase I Study and Dosing Regimen Selection to Accelerate and Inform Pivotal COVID-19 Trial of Nirmatrelvir. *Clin Pharmacol Ther* **2022,** *112* (1), 101-111.
15. Di, L.; Whitney-Pickett, C.; Umland, J. P.; Zhang, H.; Zhang, X.; Gebhard, D. F.; Lai, Y.; Federico, J. J., 3rd; Davidson, R. E.; Smith, R.; Reyner, E. L.; Lee, C.; Feng, B.; Rotter, C.; Varma, M. V.; Kempshall, S.; Fenner, K.; El-Kattan, A. F.; Liston, T. E.; Troutman, M. D., Development of a new permeability assay using low-efflux MDCKII cells. *J. Pharm. Sci.* **2011,** *100* (11), 4974-85.
16. Stopher, D.; McClean, S., An improved method for the determination of distribution coefficients. *J Pharm Pharmacol* **1990,** *42* (2), 144.
17. Walsky, R. L.; Obach, R. S., Validated assays for human cytochrome P450 activities. *Drug Metab. Dispos.* **2004,** *32* (6), 647-60.
18. Sathish, J. G.; Bhatt, S.; DaSilva, J. K.; Flynn, D.; Jenkinson, S.; Kalgutkar, A. S.; Liu, M.; Manickam, B.; Pinkstaff, J.; Reagan, W. J.; Shirai, N.; Shoieb, A. M.; Sirivelu, M.; Vispute, S.; Vitsky, A.; Walters, K.; Wisialowski, T. A.; Updyke, L. W., Comprehensive Nonclinical Safety Assessment of Nirmatrelvir Supporting Timely Development of the SARS-COV-2 Antiviral Therapeutic, Paxlovid. *Int J Toxicol* **2022,** *41* (4), 276-290.
19. Leist, S. R.; Dinnon, K. H., 3rd; Schafer, A.; Tse, L. V.; Okuda, K.; Hou, Y. J.; West, A.; Edwards, C. E.; Sanders, W.; Fritch, E. J.; Gully, K. L.; Scobey, T.; Brown, A. J.; Sheahan, T. P.; Moorman, N. J.; Boucher, R. C.; Gralinski, L. E.; Montgomery, S. A.; Baric, R. S., A mouse-adapted SARS-CoV-2 induces acute lung injury and mortality in standard laboratory mice. *Cell* **2020,** *183* (4), 1070-1085 e12.

20. Banker, M. J.; Clark, T. H.; Williams, J. A., Development and validation of a 96-well equilibrium dialysis apparatus for measuring plasma protein binding. *J. Pharm. Sci.* **2003,** *92* (5), 967-74.
21. Greenfield, S. R.; Eng, H.; Yang, Q.; Guo, C.; Byrnes, L.; Dantonio, A.; West, G.; Di, L.; Kalgutkar, A. S., Species differences in plasma protein binding of the severe acute respiratory syndrome coronavirus 2 (SARS-CoV-2) main protease inhibitor nirmatrelvir. *Xenobiotica* **2023,** *53* (1), 12-24.
22. Orr, S. T.; Ripp, S. L.; Ballard, T. E.; Henderson, J. L.; Scott, D. O.; Obach, R. S.; Sun, H.; Kalgutkar, A. S., Mechanism-based inactivation (MBI) of cytochrome P450 enzymes: structure-activity relationships and discovery strategies to mitigate drug-drug interaction risks. *J Med Chem* **2012,** *55* (11), 4896-933.
23. Walsky, R. L.; Bauman, J. N.; Bourcier, K.; Giddens, G.; Lapham, K.; Negahban, A.; Ryder, T. F.; Obach, R. S.; Hyland, R.; Goosen, T. C., Optimized assays for human UDP-glucuronosyltransferase (UGT) activities: altered alamethicin concentration and utility to screen for UGT inhibitors. *Drug Metab. Dispos.* **2012,** *40* (5), 1051-65.
24. Liu, J. B.; Xu, X. H.; Qing, F. L., Silver-Mediated Oxidative Trifluoromethylation of Alcohols to Alkyl Trifluoromethyl Ethers. *Organic letters* **2015,** *17* (20), 5048-51.
25. Owen, D. R.; Allerton, C. M. N.; Anderson, A. S.; Aschenbrenner, L.; Avery, M.; Berritt, S.; Boras, B.; Cardin, R. D.; Carlo, A.; Coffman, K. J.; Dantonio, A.; Di, L.; Eng, H.; Ferre, R.; Gajiwala, K. S.; Gibson, S. A.; Greasley, S. E.; Hurst, B. L.; Kadar, E. P.; Kalgutkar, A. S.; Lee, J. C.; Lee, J.; Liu, W.; Mason, S. W.; Noell, S.; Novak, J. J.; Obach, R. S.; Ogilvie, K.; Patel, N. C.; Pettersson, M.; Rai, D. K.; Reese, M. R.; Sammons, M. F.; Sathish, J. G.; Singh, R. S. P.; Steppan, C. M.; Stewart, A. E.; Tuttle, J. B.; Updyke, L.; Verhoest, P. R.; Wei, L.; Yang, Q.; Zhu, Y., An oral SARS-CoV-2 M(pro) inhibitor clinical candidate for the treatment of COVID-19. *Science* **2021,** *374* (6575), 1586-1593.
26. Levchenko, K.; Datsenko, O. P.; Serhiichuk, O.; Tolmachev, A.; Iaroshenko, V. O.; Mykhailiuk, P. K., Copper-Catalyzed O-Difluoromethylation of Functionalized Aliphatic Alcohols: Access to Complex Organic Molecules with an OCF2H Group. *J Org Chem* **2016,** *81* (14), 5803-13.
27. Reed, L. J.; Muench, H., A simple method of estimating fifty percent endpoints. *Am. J. Hygiene* **1938,** *27* (3), 493-497.
28. Vonrhein, C.; Flensburg, C.; Keller, P.; Sharff, A.; Smart, O.; Paciorek, W.; Womack, T.; Bricogne, G., Data processing and analysis with the autoPROC toolbox. *Acta Crystallogr. D Biol. Crystallogr.* **2011,** *67* (4), 293-302.
29. Winn, M. D.; Ballard, C. C.; Cowtan, K. D.; Dodson, E. J.; Emsley, P.; Evans, P. R.; Keegan, R. M.; Krissinel, E. B.; Leslie, A. G.; McCoy, A.; McNicholas, S. J.; Murshudov, G. N.; Pannu, N. S.; Potterton, E. A.; Powell, H. R.; Read, R. J.; Vagin, A.; Wilson, K. S., Overview of the CCP4 suite and current developments. *Acta Crystallogr. D Biol. Crystallogr.* **2011,** *67* (Pt 4), 235-42.
30. AFITT 2.6.2.2. http://www.eyesopen.com/.
31. Wlodek, S.; Skillman, A. G.; Nicholls, A., Automated ligand placement and refinement with a combined force field and shape potential. *Acta Crystallogr. D Biol. Crystallogr.* **2006,** *62* (Pt 7), 741-9.
32. Emsley, P.; Lohkamp, B.; Scott, W. G.; Cowtan, K., Features and development of Coot. *Acta Crystallogr. D Biol. Crystallogr.* **2010,** *66* (Pt 4), 486-501.

33. Bricogne, G.; Blanc, E.; Brandl, M.; Flensburg, C.; Keller, P.; Paciorek, W.; Roversi, P.; Sharff, A.; Smart, O. S.; Vonrhein, C.; Womack, T. O. *BUSTER*, 2.11.8; Global Phasing Ltd.: Cambridge, United Kingdom, 2017.
34. Weiss, M. S.; Hilgenfeld, R., On the use of the merging R factor as a quality indicator for X-ray data. *J. Appl. Crystallogr.* **1997,** *30* (2), 203-205.
35. Karplus, P. A.; Diederichs, K., Linking crystallographic model and data quality. *Science* **2012,** *336* (6084), 1030-3.
36. Brünger, A. T., Free R value: Cross-validation in crystallography. In *Methods in Enzymology*, Carter, C. W., Jr.; Sweet, R. M., Eds. Academic Press: 1997; Vol. 277, pp 366-396.